

MICROMILLING OF WROUGHT H13 TOOL STEEL

A Thesis

by

ANDREW ROBERT RUSSELL

Submitted to the Graduate and Professional School of
Texas A&M University
in partial fulfillment of the requirements for the degree of

MASTER OF SCIENCE

Chair of Committee,	Wayne Hung
Co-Chair of Committee,	Mathew Kuttolamadam
Committee Members,	Dinakar Sagapuram
Head of Department,	Reza Langari

August 2022

Major Subject: Engineering Technology

Copyright 2022 Andrew R. Russell

ABSTRACT

This paper compared performance of commercially available tool coatings for micromilling of wrought H13 tool steel in minimum quantity lubrication condition. Performance of uncoated WC-Co tool was evaluated against six different coatings -- Nano3, Uni+, TiSiNext, AlTiN, TiN, and TiAlN. Line and area surface finish of micromilled channels, and channel width were used as tool evaluating criteria. Scanning electron microscopy observation revealed the similar wear mechanism of coated microtools; the thin coating was worn out in abrasive mode following by attrition wear of the WC-Co substrate due to spalling of built-up edges and substrate. Although the measured surface finish was higher than the theoretical value, both Nano3 and Uni+ produced lowest surface finish compared to other coatings. A low cutting speed of 20m/min significantly produced lower and stable surface finish compared to those after 40 m/min cutting speed.

DEDICATION

I would like to dedicate this work to my family and friends who encouraged and inspired me throughout my years at Texas A&M. I would like to especially thank my mother Hilda Russell for being a constant source of inspiration in my life.

ACKNOWLEDGEMENTS

I would like to thank my research advisor and committee chair Dr. Hung for his guidance throughout my research, along with my committee members Dr. Kuttolamadom and Dr. Sagapuram.

Thank you also to Professor Reginaldo Coelho from the School of Engineering at São Carlos, University of São Paulo in Brazil for his help with the Directed Energy Deposition components of my research.

Finally, I would like to acknowledge Mr. Shyam Balasubramanian, Mr. Alejandro Mendez, and Ms. Sai Suri Raghava Bhargavi for their help in conducting machining experiments and Mr. Jacob Southern for his help in using the Alicona Infinite Focus Microscope. Thank you to Mr. Anthony Marino, Mr. Michael Craig, Mr. Trenton Schoonmaker, and Mr. Keelan Lindsay for their support of this project. Thank you for the support from Performance Micro Tools, Swiss-Tek Coatings, and the Microscopy and Texas A&M University Microscopy and Imaging Center Core Facility (RRID:SCR_022128).

CONTRIBUTORS AND FUNDING SOURCES

Contributors

This work was supported by a thesis committee Dr. Hung [advisor] and Dr. Kuttolamadom of the Department of Engineering Technology and Industrial Distribution and Dr. Sagapuram of the Department of Industrial and Systems Engineering.

A portion of the data analyzed in section 5.4 was provided by Sai Suri Raghava Bhargavi.

All other work conducted for the thesis was completed by the student independently.

Funding Sources

This research work is co-supported by the 2019 TAMU-FAPESP Program from Texas A&M University (USA) and the São Paulo Research Foundation (Brazil).

NOMENCLATURE

Acronyms

AISI	American Iron and Steel Institute
ANOVA	Analysis of Variance
ASTM	American Society for Testing and Materials
BJ	Binder Jetting
BUE	Built-Up-Edge
CNC	Computer Numerical Control
CSAM	Cold Spray Additive Manufacturing
DED	Directed Energy Deposition
EDS	Energy Dispersive X-Ray Spectroscopy
Lc	Low Pass Frequency Filter for Ra
MQL	Minimum Quantity Lubrication
PBF	Powder Bed Fusion
PCC	Pearson Correlation Coefficient
Ra	Line Surface Roughness
Ra'	Theoretical Surface Roughness
Sa	Area Surface Roughness
SEM	Scanning Electron Microscope
SLM	Selective Laser Melting
WAAM	Wire Arc Additive manufacturing
WC-Co	Tungsten Carbide Cobalt
Wire EDM	Wire Electrical Discharge Machining

Variables

$\text{cov}(Ra, Sa)$	Covariance of Ra and Sa
f_t	Chip Load
Ra	Line Surface Roughness
Ra'	Theoretical Surface Roughness
Sa	Area Surface Roughness
α	Concavity Angle
σ_{Ra}	Standard Deviation of Ra
σ_{Sa}	Standard Deviation of Sa

TABLE OF CONTENTS

	Page
ABSTRACT	ii
DEDICATION	iii
ACKNOWLEDGEMENTS	iv
CONTRIBUTORS AND FUNDING SOURCES.....	v
NOMENCLATURE.....	vi
TABLE OF CONTENTS	vii
LIST OF FIGURES.....	ix
LIST OF TABLES	xi
1. INTRODUCTION.....	1
2. SCOPE AND OBJECTIVE	2
3. LITERATURE REVIEW	3
3.1. H13 vs D2 Tool Steel.....	3
3.1.1. Composition	3
3.1.2. Heat Treatment and Mechanical Properties	3
3.1.3. Application	4
3.2. Metal Additive Manufacturing.....	4
3.3. Mold Repair Processes	6
3.4. Micromilling.....	7
3.4.1. Micro Versus Macro.....	7
3.4.2. Surface Roughness	8
3.4.3. Tool Coatings	9
3.4.4. Process Parameters	10
3.4.5. Use of Coolant.....	10
3.5. Machining of Wrought versus Additively Manufactured Metals	11
3.6. Research Gap.....	13
4. EXPERIMENTAL PROCEDURE	14

4.1. Tools.....	14
4.2. Materials.....	15
4.3. Equipment	15
4.3.1. Milling Machines	15
4.4. Milling Procedure.....	15
4.4.1. Workpiece Preparation	15
4.4.2. Micromilling Procedure	18
4.4.3. Metrology	19
5. RESULTS AND DISCUSSIONS	21
5.1. Preliminary Machining.....	21
5.2. Machining.....	21
5.3. Surface Finish.....	27
5.3.1. Ra versus Sa	27
5.4. Effect of Tools Coating and Cutting Speed	30
5.5. Channel Width.....	32
5.6. Coating Wear.....	33
6. CONCLUSIONS AND RECOMMENDATIONS.....	39
REFERENCES.....	40
APPENDIX A MICROMILLING PROCEDURE	47
APPENDIX B TOOL AND PART OFFSETS FOR MICROMILLING	49
APPENDIX C NC CODES.....	51
APPENDIX D PROCEDURE USING ALICONA INFINITE FOCUS MICROSCOPE	52

LIST OF FIGURES

	Page
Figure 1: Tool Identification in a Toolbox	14
Figure 2: Using an indicator to measure parallelism 1) Indicator, 2) Workpiece, and 3) Granite Reference Block	16
Figure 3: Workpiece and Setup for Micromilling: 1. Micromill, 2. MQL Nozzle, 3. Workpiece.....	17
Figure 4: Tool Path for Micromilling, Unit: mm, Not to Scale	18
Figure 5: Concavity Angle of an Uncoated Tool	20
Figure 6: Surface Finish, Ra, for First 1000 mm. Depth of Cut: 40 μm , Cutting Speed: 40 m/min, Chip Load: 10 $\mu\text{m}/\text{flute}$	21
Figure 7: Averaged Ra and ranges for first 20 mm. Depth of Cut: 40 μm , Cutting Speed: 40 m/min, Chip Load: 10 $\mu\text{m}/\text{flute}$	22
Figure 8: Feed Diagram showing Up-milling and Down-milling.....	24
Figure 9: SEM photo of channel machined using Nano3 coated tool a) Center of the channel and b) edge of the channel.....	25
Figure 10: Ra in middle vs edge of channel. Depth of Cut: 40 μm , Cutting Speed: 40 m/min, Chip Load: 10 $\mu\text{m}/\text{flute}$	26
Figure 11: Ra and Sa versus cutting length for coatings. Depth of Cut: 40 μm , Cutting Speed: 40 m/min, Chip Load: 10 $\mu\text{m}/\text{flute}$	29
Figure 12: Ra of Machined Channels at Different Cutting Speeds. Depth of Cut: 40 μm , Cutting Speed: 40 m/min and 20 m/min, Chip Load: 10 $\mu\text{m}/\text{flute}$	30
Figure 13: Effects of Coating on Channel Width. Depth of Cut: 40 μm , Cutting Speed: 40 m/min, Chip Load: 10 $\mu\text{m}/\text{flute}$	33
Figure 14: Uncoated cutting edges after machining 141 mm. Depth of Cut: 40 μm , Cutting Speed: 40 m/min, Chip Load: 10 $\mu\text{m}/\text{flute}$	35
Figure 15: Nano3 Coated cutting edges after machining 23 mm. Depth of Cut: 40 μm , Cutting Speed: 40 m/min, Chip Load: 10 $\mu\text{m}/\text{flute}$	35

Figure 16: AlTiN Coated cutting edges after machining 23 mm. Depth of Cut: 40 μm , Cutting Speed: 40 m/min, Chip Load: 10 $\mu\text{m}/\text{flute}$	36
Figure 17: TiAlN Coated cutting edges after machining 141 mm. Depth of Cut: 40 μm , Cutting Speed: 40 m/min, Chip Load: 10 $\mu\text{m}/\text{flute}$	36
Figure 18: TiN Coated cutting edges after machining 23 mm. Depth of Cut: 40 μm , Cutting Speed: 40 m/min, Chip Load: 10 $\mu\text{m}/\text{flute}$	37
Figure 19: TiSiNext Coated cutting edges after machining 23 mm. Depth of Cut: 40 μm , Cutting Speed: 40 m/min, Chip Load: 10 $\mu\text{m}/\text{flute}$	37
Figure 20: UNI+ Coated cutting edges after machining 23 mm. Depth of Cut: 40 μm , Cutting Speed: 40 m/min, Chip Load: 10 $\mu\text{m}/\text{flute}$	38
Figure 21: Using a bullet level (Top View) 1) Bullet Level and 2) Compound Vise	47
Figure 22: Using Indicator Mounted to the Spindle 1) Indicator, 2) Workpiece, 3) Magnetic Mounting Base, and 4) Compound Vise	48
Figure 23: Using Laser Height Gage 1) Magnetic Mounting Base, 2) Laser Height Gage, and 3) Washer with aluminum sheet	50

LIST OF TABLES

	Page
Table 1: Element Composition of H13 and D2 Tool Steels (wt%) [1]	3
Table 2: Microhardness of wrought and DED deposited H13 and D2 tool steels [25]....	12
Table 3: Tool Coating Three Letter Codes.....	14
Table 4: Parameters for each stage of Machining	17
Table 5: Average Ra of Machined Surface for the first 20 mm of cutting length of different tools.....	23
Table 6: Pearson Correlation Coefficient between Ra and Sa of the machined surface after 20 and 138 mm of cutting length.....	28
Table 7: Machining Parameters of other researchers	31

1. INTRODUCTION

Molds and dies used for mass production are a large investment that will eventually degrade or get damaged during their life. Replacing a mold is costly so repair is usually preferred, but this requires long lead times and can cause production down time. The current most common method of repair consists of using welding to fill cracks in the mold, heat treating the mold, then using machining to reshape the mold. This is a costly process that has downsides, such as the difficulty to machine the hardened tool steel that is commonly used in molds.

This research is part of a larger project to repair molds and dies using a combination of Directed Energy Deposition (DED) and micromilling. DED allows for cracks in the workpiece to be filled using the same material as the workpiece. Micromilling will then be used because it can be used for reshaping materials deposited by DED.

This project is specifically looking to find the optimal micromilling parameters and the best coating for wrought H13 tool steel, which is a commonly used mold and die material. These results will then be used in a future project to compare with DED created material.

2. SCOPE AND OBJECTIVE

The objective of this research is to optimize the micromilling of mold material by studying:

- Tool Coating
- Tool Life
- Surface Finish
- Cutting Parameters

The scope of this research includes:

- Selecting square end milling tools without coating and commercially coated with AlTiN, Nano3, TiAlN, TiN, TiSiNext, and Uni+
- Using wrought unhardened H13 tool steel
- Varying cutting speed while maintaining a specific and practical chip load and depth of cut
- Studying tool performance by slot quality
- Using Minimum Quantity Lubrication (MQL) as cutting fluid during micromilling

3. LITERATURE REVIEW

As the world has an increased need for more miniaturized products, micromilling has provided a way for creating the miniature products or the dies and molds for creating those products.

3.1. H13 vs D2 Tool Steel

H13 and D2 tool steels are both commonly used in a range of mold and die applications.

3.1.1. Composition

There is a large difference in the chromium and carbon percentage that leads to differences in machinability of the steels. The higher amount of chromium and carbon lead to higher hardness in the material which gives it better wear resistance but also makes machining more difficult. D2 tool steel has a hardness of about 58 HRC while H13 tool steel has a hardness of about 52 HRC.

Table 1: Element Composition of H13 and D2 Tool Steels (wt%) [1]

Tool Steel	C	Mn	Si	Cr	Ni	Mo	V
H13	0.32-0.45	0.2-0.5	0.8-1.2	4.75-5.50	0.3	1.1-1.75	0.8-1.2
D2	1.40-1.60	0.6	0.6	11.0-13.0	0.3	0.7-1.2	1.1

3.1.2. Heat Treatment and Mechanical Properties

Standard heating treating procedure for H13 tool steel is heated to 1050°C then quenched and tempered at 600°C from 15 minutes to multiple hours to achieve different hardness depending on the desired results [2]. Generally, the longer the tempering time the lower the hardness. Barhami et al. (2005) found that after 90 minutes of tempering

there was a temporary increase in hardness from 35 HRC to 45 HRC that was attributed to carbide precipitations.

3.1.3. Application

D2 is a cold work steel used in applications such as cold forming molds, deep drawing molds, and cold rolling reels [3]. It's high toughness and wear resistance give it good dimensional stability in high production applications. H13 is a hot work steel used in applications such as hot forging dies, hot extrusion channels, and high-pressure dies due to its high hardness and resistance to high-temperature fatigue and wear [4].

3.2. Metal Additive Manufacturing

Metal additive manufacturing provides a way to make parts with unique structures and geometries that are not possible through traditional manufacturing techniques. There are many different methods of metal additive manufacturing that all have their advantages and disadvantages.

In Binder Jetting (BJ), droplets of a binder are deposited onto a powder bed to join particles and then the binder is cured. This is done layer by layer to build up the part. The biggest advantage of binder jetting is that it can be used with almost any powder, such as ceramics, metals, and polymers [5]. When used for metal additive manufacturing, after curing the part is sintered to increase its strength [6].

In Wire Arc Additive Manufacturing (WAAM), welding wire is used as the deposited material and an electrical arc is used as the heat source [7]. The process involves depositing layer by layer of material to build up the part and can be done on any work surface. This process has a very high material deposition rate making it quicker to

make large parts. The downside of this process is that the layer thickness is dependent on the size of available welding wire, with typical layer heights between 1 and 2 mm. This means it cannot be used for small or high precision parts.

Cold Spray Additive Manufacturing (CSAM) consists of spraying particles at very high speed into a substrate to cause plastic deformation and bonding [8]. The advantages of this process are a short production time, high flexibility of uses, and low thermal effects. It can be used for surface treatment and surface defect repair. It does, however, lead to high surface roughness, low dimensional accuracy, and high porosity.

Powder Bed Fusion (PBF) uses a thin layer of powder then fuses it with the heat source, such as a laser or electron beam. Another layer of powder is added on top, and the process is repeated to build the part. This results in a part that has high dimensional accuracy and usually only needs minimal post-processing. A downside of powder bed fusion is that the part must be built within the powder bed, so there is a limitation on the size of the part being made and it cannot be built on an existing workpiece because it requires a flat surface for the layer of powder. One of the more common forms of this process is Selective Laser Melting (SLM).

In DED, a wire or powder is fed to where the heat source contacts the work surface. This allows for dimensional freedom as the material can be deposited only where it is needed and does not require a powder bed. It has an inferior level of dimensional accuracy as PBF and requires more post-processing. The ability to deposit material locally by the DED process makes it ideal for mold repairing.

The use of DED does provide some challenges that must be accounted for. One of the issues with DED created H13 tool steel parts is that the deposited steel has a higher hardness value than wrought H13 steel [9]. Park et al. (2016) studied the effect of energy input on the hardness of H13 and D2 tool steels deposited by the directed metal tooling process, which was based on DED. They found that the hardness of both metals decreased with an increase of input energy. This was attributed to both a change in microstructure from the increased energy and a decrease in carbon in the deposited material. The deposited D2 steel had a lower hardness than the wrought D2 steel. This was attributed to the different microstructures formed in DED process. Deposited D2 steel formed an entirely dendritic structure compared to the martensitic structure of the wrought D2 steel which led to the difference in hardness [9].

3.3. Mold Repair Processes

Traditional mold repair techniques mainly rely on some form of welding to fill cracks. This can lead to part damage due to the heat affected zone. A technique using a combination of laser cladding and milling was proposed by Jeng et al. (2001)[10]. They were able to add to an existing mold using laser cladding and then use milling to accurately resize the new material, but at the time did not deem the process a feasible way to perform mold repair due to the high layer thickness of the laser cladding process. Zhang et al. (2019) proposed a method of mold repair using a combination of DED and milling but reversed the order of the operations from that performed by Jeng et al [10], [11]. They started by milling away the damaged section of the mold and then refilling it

using DED to restore the original dimensions. They found that by heat treating the mold they had strong bonding between the mold and the deposited material.

3.4. Micromilling

3.4.1. Micro Versus Macro

While the basic concepts of machining are transferable from macromilling to micromilling, there are new challenges presented as the size of the tool decreases as discussed by Chae et al. (2006) [12]. The size of the tools means that even small vibrations can have a large effect on tool life and machining accuracy. It can also be difficult to detect defects on the tool.

The ratio of cutting-edge radius to undeformed chip thickness becomes much more critical when micromilling. Many different ratios have been presented by Oliveira et al. (2015) ranging from 0.14-0.40 [13]. This range was dependent on the tool and workpiece materials. Aramcharoen et al. (2009), who studied micromilling of H13 tool steel, tested ratios from 0.2-2.0 and found that the best ratio of undeformed chip thickness to cutting edge radius was 1.0 [14].

Tool runout is another concern that arises when micromilling. While the effects are negligible when macromachining, the combination of spindle runout and small diameter of the cutting edge can lead to poor surface finish or catastrophic tool failure. Wang et al. (2020) studied tool runout and found that surface roughness increased with tool runout and that runout can lead to “single-tooth cutting” [15]. With a two-flute end mill, “single-tooth cutting” can lead to a high surface roughness and a shortened tool life. Oliaei et al. (2016) also found that uneven tool wear can have results that appear

like tool runout [16]. As one cutting edge experiences more wear than the other, the tool may begin to experience single tooth cutting and a high surface finish. Their recommendation was to have a radial immersion of 60% to help balance the cutting-edge wear.

3.4.2. Surface Roughness

Davoudinejad et al. (2020) studied tool wear in the micromilling of nitride hardened tool steel and found that surface finish went from rough to smooth and back to rough as tool wear progressed [17]. They found that there was a high initial surface roughness coming from scratches that were left on the surface from the new tool, but after a certain amount of tool wear the more rounded cutting edge of the tool led to a smoother surface finish for a short period of time until excess tool wear caused another increase in surface roughness. Muhammad et al. (2021) found that cutting speed was the most important parameter for minimizing surface roughness when machining Inconel 718, with 48% of the variability [18]. They also found that tool coating had a minimal effect on the surface roughness, with a contribution percentage of about 10%.

Hassanpour et al. (2016) found that spindle speed was an even more influential parameter with 94.8% of the variability when machining Ti6Al4V [19].

Varghese et al. (2019) studied the relationship between surface roughness and tool-life in micromilling of 304 stainless steel [20]. Their experiment involved using their tools until breakage and studying the surface roughness of the channel at different points. They found that the tool life had three distinct stages. The first 15% of the tool life had high variation in the surface roughness, which was attributed to the tool chipping

as it made initial contact with the workpiece. The second stage that went until about 50% of the cutting length had a constant surface roughness. The last stage of tool life then saw an increase in surface roughness before the tool broke. They also identified two types of tools, those with similar cutting-edge radii and those that had one sharp and one rounded cutting radii. They observed that the tools with type similar cutting-edge radii had a lower tool life but also a lower surface finish, while the tools with different radii had more than double the cutting length but had a higher surface finish.

3.4.3. Tool Coatings

Tool coatings extends the life of tools in conventional machining operations. Due to the differences, it is important to see if there are differences in how tool coatings affect machining characteristics in micromilling. Muhammad et al. (2021) studied the effects different machining parameters, including tool coatings, had on the micromilling of Inconel 718 [18]. They found that tool coating was not a significant parameter in burr formation and surface roughness, with a contribution percentage of about 10%. This may be because they used of a cutting length of 10 mm. Aramcharoen et al. (2008) found that coatings had a “burn-in-period” where there was no difference between them [21]. With a longer cutting length Muhammad et al. may have found a larger difference.

Aramcharoen et al. compared an uncoated tool to TiN, CrN, TiCN, TiAlN, and CrTiAlN coated tools for the micromilling of H13 tool steel without any cutting fluid. They found that all the coatings helped to reduce cutting edge chipping and edge radius wear. TiN and CrTiAlN coatings both helped to reduce flank wear. They found that the TiN coated tool performed the best based on flank wear, surface finish, and burr size.

3.4.4. Process Parameters

Manso et al. (2020) investigated how different machining parameters affected surface roughness in the micromilling of H13 tool steel [22]. They studied feed per tooth, spindle speed, and cutting length. They found that a feed per tooth of 2 μm had the lowest initial surface roughness with an Rz value of 174 nm after a cutting length of less than 200 mm, but after 1200 mm the surface roughness was the highest with an Rz value of 423 nm. With a feed per tooth of 4 and 5 μm the surface roughness was higher initially, with an Rz value around 500 nm but reduced quickly and leveled out between 200 and 300 nm for the rest of the cutting length. They also found that increasing spindle speed led to better surface quality.

3.4.5. Use of Coolant

The use of coolant in machining is important for evacuating chips, lubricating the tool, and dissipating heat. Traditional techniques of providing coolant are not possible because the force from the cutting fluid can be higher than the cutting forces. This can lead to tool deflection and damage that will cause poor machining results. Dry machining can be done but has issues with poor tool life and high heat. Minimum quantity lubrication (MQL) is an effective way of providing enough coolant to be effective without deflecting or damaging the tool by propelling micron sized lubricant within an airjet. In their study, Vazquez et al. (2015) compared dry machining, conventional emulsion cooling, and MQL in the micromilling of Ti6Al4V titanium [23]. They found that the use of MQL led to less tool wear and a less error in the shape of the channel. Ziberov et al. (2016) compared MQL to dry machining for micromilling of

Ti6Al4V titanium and found that MQL led to a better surface finish[24]. However, they observed that dry machining provided a better tool life. They attributed this to built-up-edge (BUE) protecting the tool's cutting edges.

3.5. Machining of Wrought versus Additively Manufactured Metals

Park et al. (2016) studied the effects of heat treatment on wrought and DED produced H13 and D2 tool steels [25]. The produced samples by depositing steel directly onto a heat-treated substrate of the same type of steel using an energy input of 37.81 J/mm² and a scan rate of 14.7 mm/s. The hardness of the steels before and after heat treatment is shown in Table 2. Before heat treatment deposited H13 had a higher hardness than wrought H13, while deposited D2 had a lower hardness than wrought D2, but after heat treatment both steels had similar hardness between wrought and deposited. The difference in initial hardness was attributed to a difference in microstructure caused by the rapid cooling rate of the DED process. After heat treatment deposited H13 had a similar microstructure to wrought H13, while deposited D2 was different to wrought D2, although they had the same hardness. Initially the deposited H13 was made up mostly of ferrite and austenite, but after heat treating it became tempered martensite like the wrought H13. In contrast the deposited D2 consisted of dendritic and eutectic structures which transformed into fine carbides in tempered martensite after heat treating, compared to the large carbides in tempered martensite that is found in wrought D2 steel. Wrought D2 steel is generally produced through a forging process that leads to its coarse carbides being parallel to the forging direction leading to anisotropic properties. The heat

treated deposited D2 steel had its fine carbides distributed uniformly distributed meaning it should have isotropic properties.

Table 2: Microhardness of wrought and DED deposited H13 and D2 tool steels [25]

	Wrought H13	DED H13	Wrought D2	DED D2
Before Heat Treatment (VHN)	499±6	630±5	643±14	470±10
After Heat Treatment (VHN)	528±5	535±5	719±7	745±3

Koshy et al. (2002) compared the macro milling of H13 and D2 steel with no cutting fluid. The H13 tool steel had a hardness of 52 HRC, while the D2 tool steel had a hardness of 58 HRC [1]. They found that D2 steel had much higher machining temperatures, 700°C, compared to H13 which was between 200 and 400°C at a cutting speed of 200 mm/min. They found that with a cutting speed of 150 m/min, the cutting length increased from 15 m to 250 m for machining of H13 tool steel. This was done using a tool coated with TiCN with an upper coating of TiN.

Sadiq et al. (2018) compared the micromilling of SLM created Inconel 718 in MQL to wrought material, the authors found that the SLM formed harder carbide particles which are more difficult to machine [26]. Bai et al. (2020) compared the macro milling of both DED'ed and hot-rolled A131 steel [27]. They found that at a cutting speed of 150 m/min, the tool wear was the same between the DED'ed and hot-rolled samples, but as the cutting speeds increased to 250 m/min the tool wear was more severe from milling the hot-rolled sample. The tool wear depth for the DED samples were 13.55 and 16.36 µm, while the tool wear depth for the hot-rolled sample was 27.15 µm.

3.6. Research Gap

The micro-milling of wrought tool steel has been studied but there has been limited information on the micro-milling of additively manufactured H13 tool steel. It is important to have a good understanding of how the specific tool coatings perform when machining wrought H13 steel so that they can be better evaluated when used on the DED deposited steel. This research studies the machinability of wrought H13 tool steel for comparison in a parallel study of the machinability of DED deposited H13 tool steel.

4. EXPERIMENTAL PROCEDURE

4.1. Tools

The cutting tools used were two-flute micro end mills with a diameter of 0.4 mm acquired from Performance Micro Tool [34] with a flute length of 0.5842 mm. The six types of coatings acquired from Swiss-Tek Coatings [35] were Uncoated, Nano3, Uni+, AlTiN, TiAlN, TiN, and TiSiNext for comparison against uncoated tools. Each of the coatings were given a three-letter code, shown in Table 3, and each tool was identified by its row and column in the box, as shown in Figure 1, to make identification easier.

Table 3: Tool Coating Three Letter Codes

Uncoated	Nano3	Uni+	AlTiN	TiAlN	TiN	TiSiNext
UNC	NAN	UNI	ALT	TIA	TIN	TIS

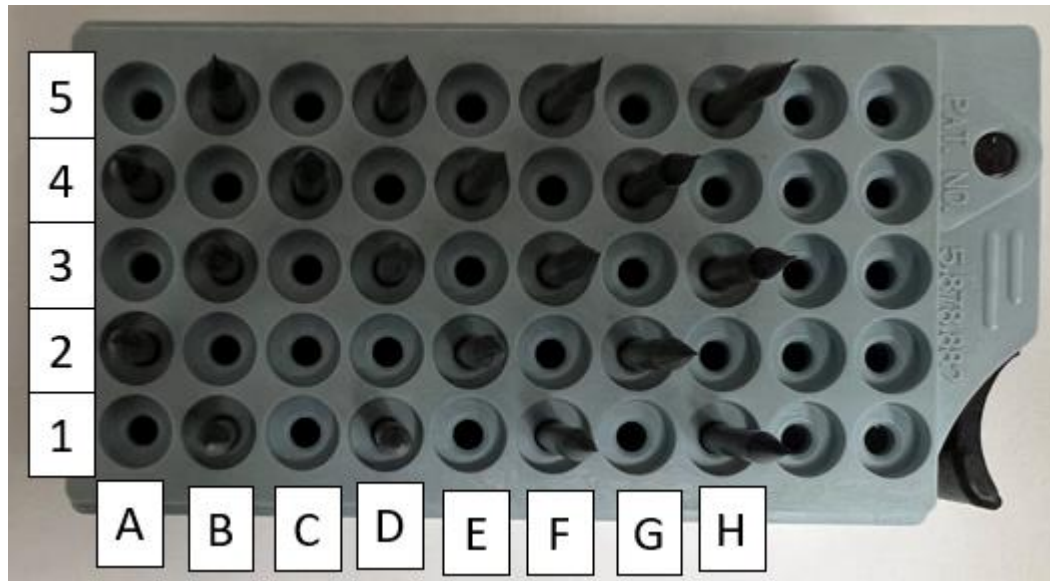


Figure 1: Tool Identification in a Toolbox

4.2. Materials

The workpiece was H13 Tool Steel with an averaged hardness of 86 HRB. The hardness of the workpiece was recorded using a Wilson Rockwell Hardness Tester model 3JR. The dimensions of the workpiece were 107x82x47 mm. The composition of the H13 Tool Steel is shown in Table 1 and a tensile strength of 1569 MPa [36].

4.3. Equipment

4.3.1. Milling Machines

The Haas VF1 CNC mill was used to machine the workpiece for parallelism and to minimize damage to the new surface for micromilling. The Haas OM2 CNC mill was used for micro milling operations with an air bearing spindle that allows for speeds of up to 50,000 rpm.

Flood cooling was used for the Haas VF1 mill, while a UNIST cool lubricator system with a needle nozzle was used in the Haas OM2 mill. The UNIST system provided micromist cooling and lubrication of the tool and workpiece at a rate of 0.084 mL/min using Coolube 2210 EP.

4.4. Milling Procedure

4.4.1. Workpiece Preparation

The first step was to machine the workpiece for parallelism. The Haas VF1 mill was used to face the workpiece with a depth of cut of 0.0762 mm and a cutting speed of 40 m/min. This process was repeated until a uniform surface finish was made across the surface of the part and was repeated for both sides of the part. This required 11 passes on one side and 9 passes on the other. An Aerospace brand dial indicator with a resolution

of 0.0254 mm (0.001 in) was then used to verify that the parallelism was within ± 0.0254 mm (± 0.001 in) as shown in Figure 2.

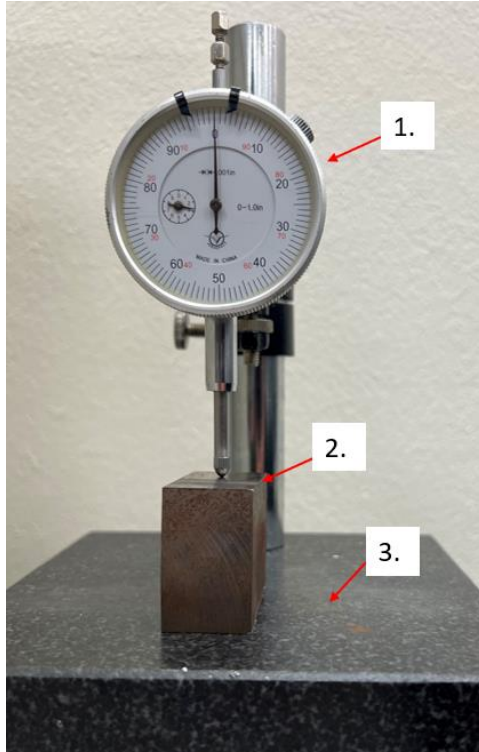


Figure 2: Using an indicator to measure parallelism 1) Indicator, 2) Workpiece, and 3) Granite Reference Block

Before machining the microtools were imaged using the Olympus STM 6 microscope to look for any tool damage.

The NC-code program shown in Appendix C was then written. Each operation would machine 5 slots into the workpiece with a 0.1 mm gap between slots. The workpiece had a width of ≈ 45 mm so the program was written to start 3 mm before the workpiece and then machine for 51 mm. This was to ensure that the tool would machine through the entire width. A sketch of the tool path is shown in Figure 4. The block was only machined from one direction to ensure that the MQL was always aligned behind to

tool to ensure that it was being applied where the cutting tool met the workpiece as shown in Figure 3. The program was then tested by machining with a wax block to verify its proper function. Three stages of machining were performed with the parameters shown in Table 4.

Table 4: Parameters for each stage of Machining

	Depth of Cut (μm)	Cutting Speed (m/min)	Chip Load ($\mu\text{m}/\text{flute}$)	Total Cutting Length (mm)
1 st Stage	40	40	10	960
2 nd Stage	40	40	10	141
3 rd Stage	40	40	10	23
4 th Stage	40	20	10	23

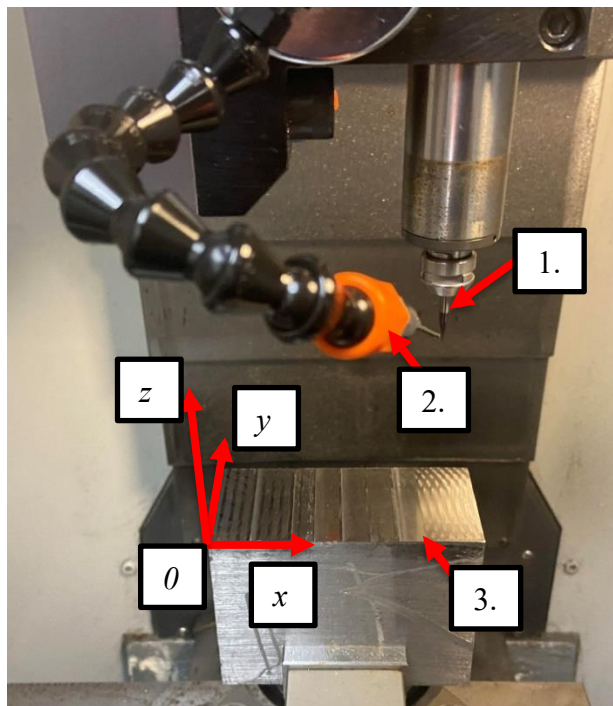


Figure 3: Workpiece and Setup for Micromilling: 1. Micromill, 2. MQL Nozzle, 3. Workpiece

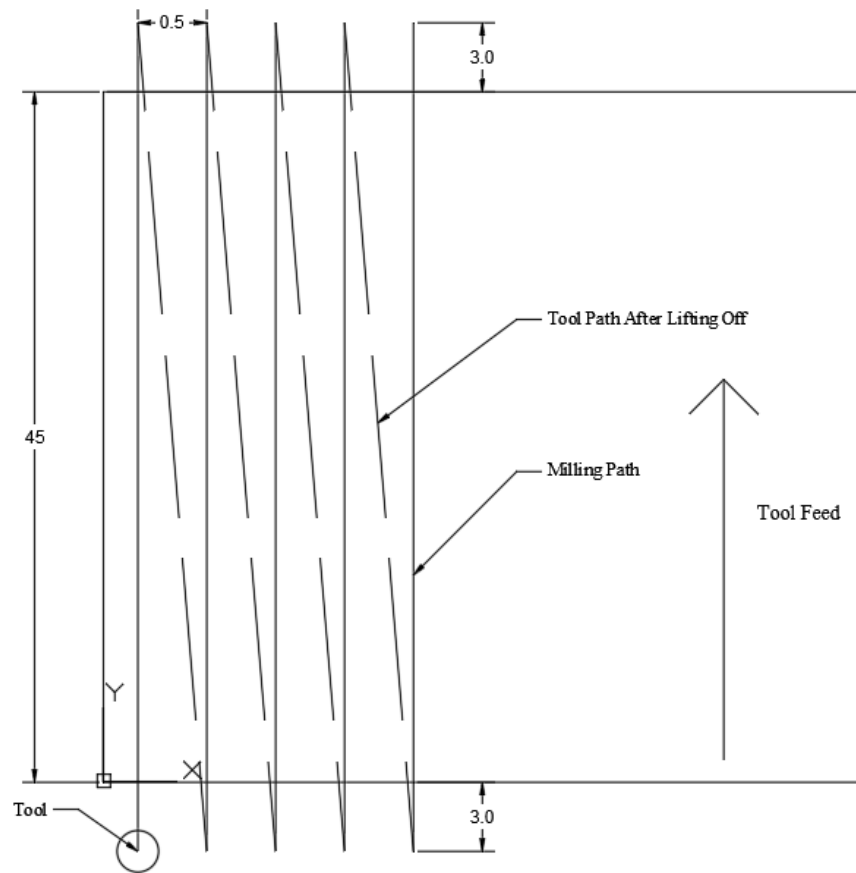


Figure 4: Tool Path for Micromilling, Unit: mm, Not to Scale

4.4.2. Micromilling Procedure

4.4.2.1. First Micromilling Test

The workpiece was secured in the compound vise on the Haas OM2 mill. A leveling plate was used to make the surface of the part parallel to the bed of the mill. An indicator mounted to the spindle was then used to verify this parallelism. The tool offsets were set, and the program was run. Details of this process are shown in Appendix A. A coated tool was tested for 20 slots. An additional tool with AlTiN coating was tested because of early tool failure after 15 slots.

After this, the process was repeated using a new tool offsetting method described in Appendix B.

4.4.2.2. Second and Third Micromilling Test

A small piece of the workpiece, with dimensions of 47x39x23 mm was cut off from the larger block using both a horizontal band saw and a wire electrical discharge machine (wire EDM). This also allowed the workpiece to fit into the Scanning Electron Microscope (SEM) chamber for further study.

The second stage of testing was then performed using the same procedures as the previous one except for the shorter cutting length of 141 mm. Afterwards, a third stage was performed using a cutting length of 23 mm. See Appendices A and B for details on the machining procedure.

4.4.2.3. Fourth Micromilling Test

A third round of milling was done using the Nano3 and UNI+ coated tools at a cutting speed of 20 m/min to study the effect of cutting speed on surface roughness. The same machining procedures from the second micromilling test was used.

4.4.3. Metrology

Surface characterization was done using the Alicona Infinite Focus Microscope. Images were taken using the Olympus STM 6 Microscope, and the Tescan Vega Scanning Electron Microscope (SEM).

The micro milled samples were studied with the SEM. The beginning and end of each channel was imaged, and energy-dispersive x-ray spectroscopy (EDS), using Oxford EDS detector, was used to detect if any tool coating deposited on the milled

slots. An uncoated tool and a tool of each coating were imaged using the SEM and EDS was performed to confirm the coating elements.

The channel's surface finish was measured with the Alicona. The procedure is shown in Appendix D. The line roughness, Ra, measurements were taken along a 1 mm long line at the center of a channel. To find the Ra value the Alicona was calibrated for the correct cutoff frequency (Lc) for each lens. This was done using a calibration piece with a known Ra value made by Mitutoyo Standard, Serial No. 348451205. The surface roughness, Sa, readings were taken from a 1x0.2mm area in the center of the channel and at every millimeter along the cutting length.

The line roughness of the center and edges of the channels at 1, 12, and 22 mm of cutting length was also recorded. The width of the channels was measured using the Alicona's form measurement function. The concavity angle of both an uncoated and Nano3 coated tool was measured using the measurement function on the Olympus STM 6 Microscope as shown in Figure 5.

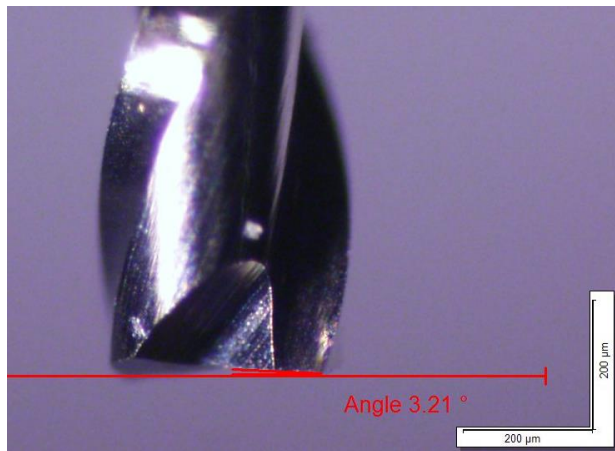


Figure 5: Concavity Angle of an Uncoated Tool

5. RESULTS AND DISCUSSIONS

5.1. Preliminary Machining

The preliminary machining was a 960 mm cutting length with different coated tools. Graphing the Ra values of the milled surface against cutting length, as shown in Figure 6, reveals that higher Ra values begin between 20 and 30 mm of cutting length depending on the coating, indicating significant tool wear. Using this information, the coatings were compared for their first 20 mm of use to ensure that they were studied within their effective tool life.

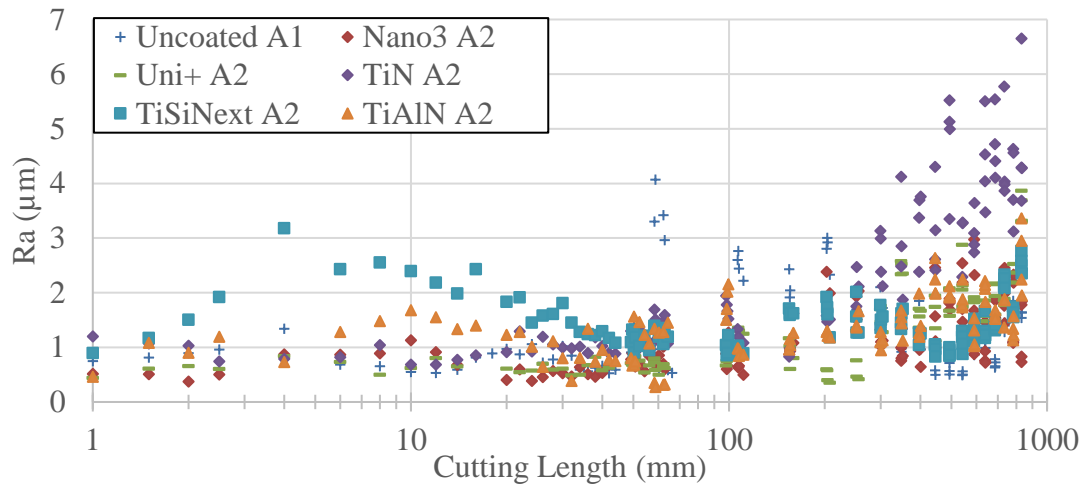


Figure 6: Surface Finish, Ra, for First 1000 mm. Depth of Cut: 40 µm, Cutting Speed: 40 m/min, Chip Load: 10 µm/flute

5.2. Machining

Figure 7 shows a comparison of the first 20 mm of cutting distance for all the tools used. The Uncoated, Nano3, AlTiN, and UNI+ had very consistent performance between the tools. TiN and TiSiNext had more variability between tools with some performing well and others performing poorly.

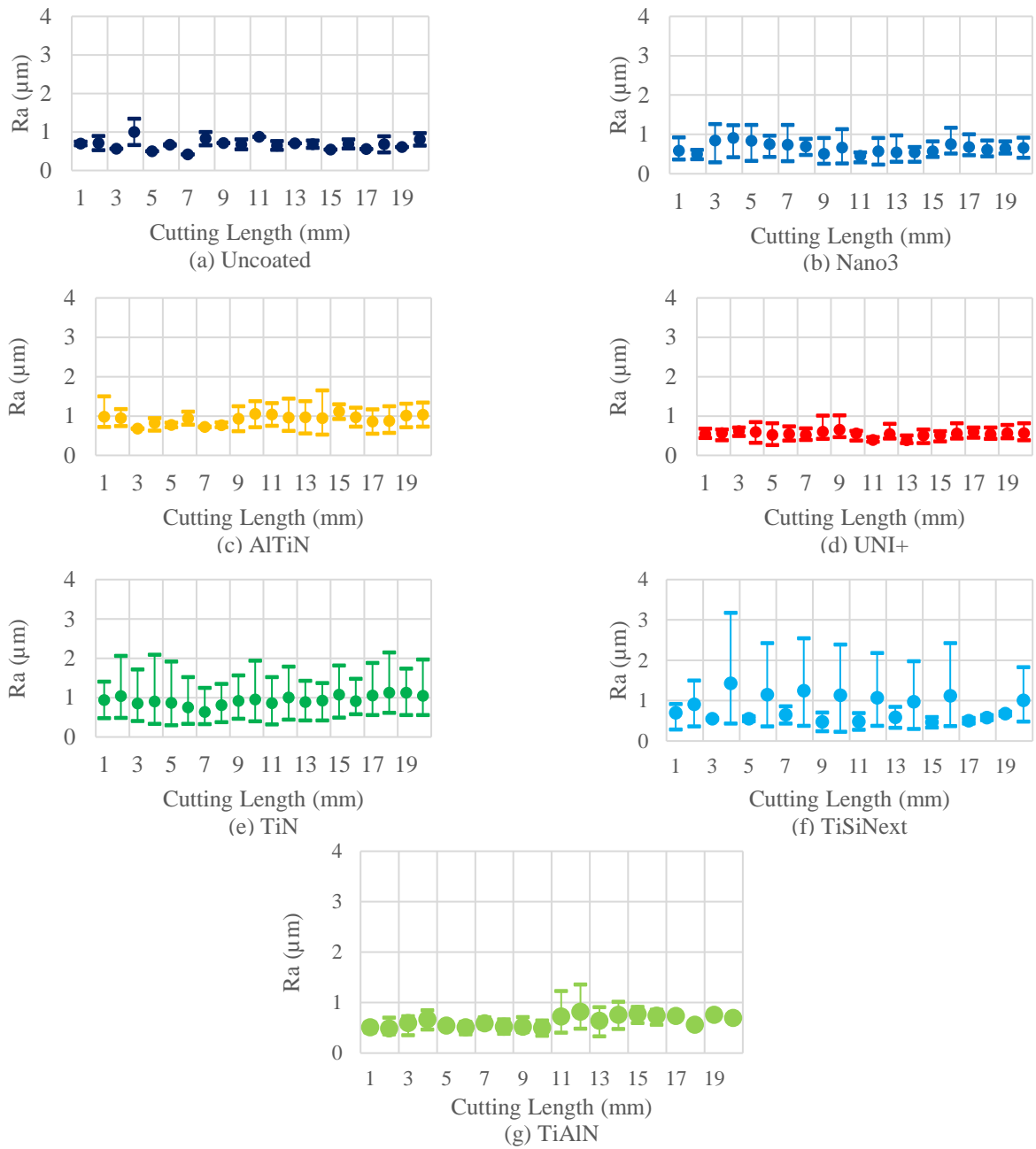


Figure 7: Averaged Ra and ranges for first 20 mm. Depth of Cut: 40 μm, Cutting Speed: 40 m/min, Chip Load: 10 μm/flute

Studying the average Ra values of the machined surface after using all the tools in Table 5, Nano3 and UNI+ has the lowest average Ra values and no obvious outlier tools. The Uncoated tools had the third lowest average Ra values but also only had two tools used due to having a limited number available. The TiSiNext coated tools had good performance from two of the tools but had one large outlier that brought up its average. The fourth tool had an issue with the tool offset that meant the data was not usable. The TiAlN coated tools were in the middle of the pack but had the only tool breakage, tool B3, which most likely would have brought up its average if it had continued due to the sharply increasing Ra values.

Table 5: Average Ra of Machined Surface for the first 20 mm of cutting length of different tools

Tool #	Uncoated	Nano3	AlTiN	UNI+	TiN	TiSiNext	TiAlN
1	0.786	0.736	0.956	0.652	0.878	2.137	1.204
2	0.649	0.455	0.870	0.499	1.699	0.395	0.680
3		0.866	1.164	0.661	0.664	0.701	0.733
4		0.595	0.694	0.426	0.469		0.505
Average Ra (μm)	0.725	0.648	0.921	0.559	0.928	1.078	0.780

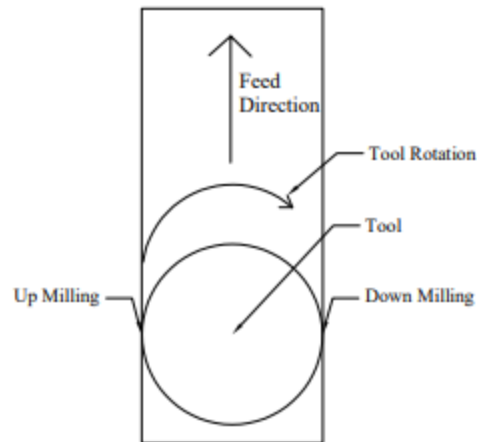
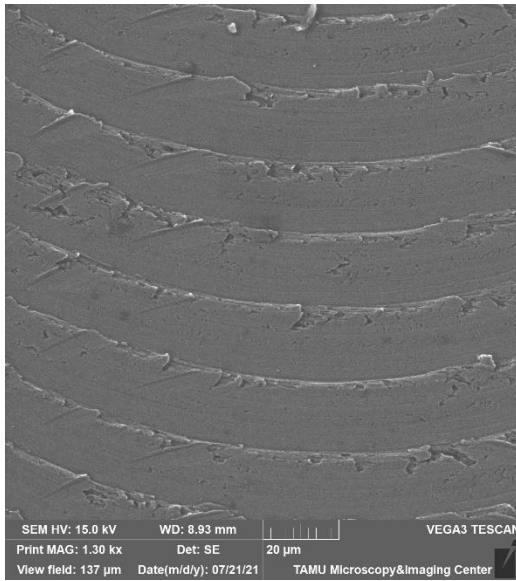
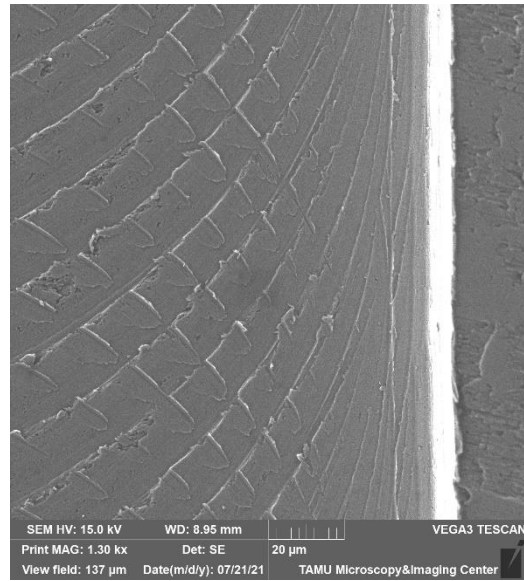


Figure 8: Feed Diagram showing Up-milling and Down-milling

The directions of up milling and down milling are shown in Figure 8. Figure 9 shows the difference in the channel at the center versus at the edge after ≈ 20 mm of cutting distance. It can be observed that at the edge of the channel the surface appears much smoother than near the center. A comparison of the Ra value between the middle of the channel and $10 \mu\text{m}$ from the edge of the channel along the cutting distance was also performed and the results are shown in Figure 10. From these results it can be determined that the middle of the channel always has a higher surface roughness than the edges. Generally, down-milling while provides a better surface finish than up-milling [37], but this data shows that up milling and down milling are very similar with no consistency on which is greater than the other. This is because the bad surface finish in up-milling is caused by the tool vibrating against the work piece as it cuts. In this case the tool is both up-milling and down-milling at the same since the tool is contained in the milled slot with minimal vibration.



(a)



(b)

Figure 9: SEM photo of channel machined using Nano3 coated tool a) Center of the channel and b) edge of the channel

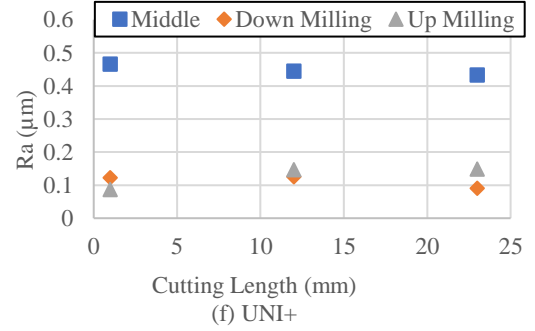
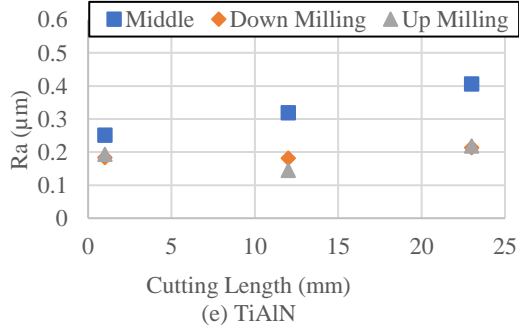
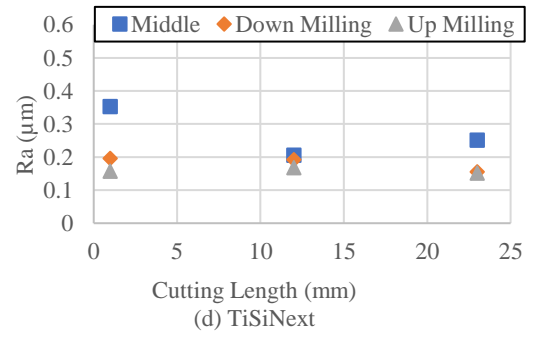
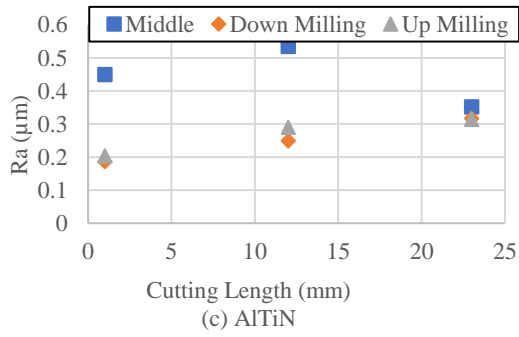
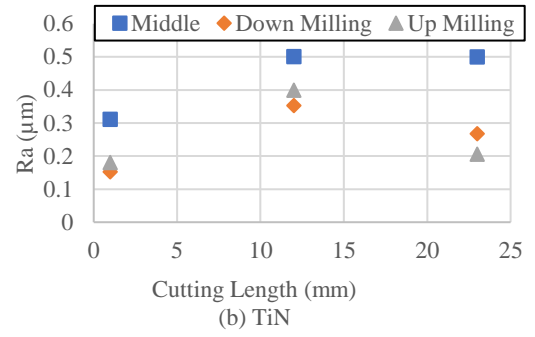
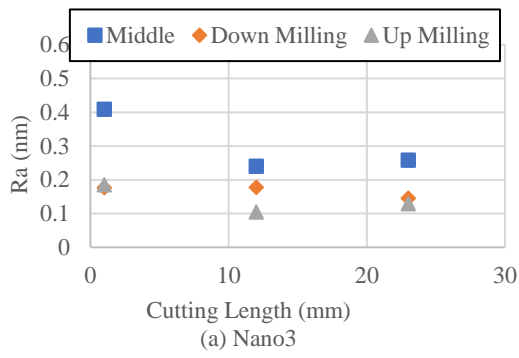


Figure 10: Ra in middle vs edge of channel. Depth of Cut: $40 \mu\text{m}$, Cutting Speed: 40 m/min , Chip Load: $10 \mu\text{m/flute}$

5.3. Surface Finish

5.3.1. Ra versus Sa

The first step after collecting the data to find if there was a relationship between Ra and Sa. The first 20 and 138 mm of cutting distance for each tool coating was compared using a moving average of the data to lessen the impact of any large outliers.

$$PCC = \frac{cov(Ra, Sa)}{\sigma_{Ra}\sigma_{Sa}} \quad (1)$$

Where:

PCC	: Pearson Correlation Coefficient
$cov(Ra, Sa)$: Covariance of Ra and Sa
σ_{Ra}	: Standard Deviation of Ra
σ_{Sa}	: Standard Deviation of Sa

The Pearson Correlation Coefficient (PCC), defined in Equation 1 [38], between Ra and Sa of the machined surfaces for each coating is shown in Table 6. This value shows how close to a linear relationship Ra and Sa have; a higher PCC value means a more linear relationship. Nano3, AlTiN, and UNI+ show a strong positive relationship, while TiAlN and TiSiNext show a moderate positive relationship. TiN shows a negligible relationship between Ra and Sa. The differences between Ra and Sa are likely caused by the higher variation in Sa values that comes from taking readings over a larger rectangular area compared to the profile reading of Ra.

Over the first 20 mm there is less correlation between Ra and Sa for Nano3, TiAlN, TiSiNext, and UNI+. This is likely because this is the region where the tool coating is worn out, causing more variation over the surface of the part. The AlTiN correlation goes down over the longer cutting distance, but this is likely caused by the

comparatively high variation in Ra after 50 mm, shown in Figure 11b. TiN has a negligible correlation between Ra and Sa for after both cutting lengths that appears to be caused by the unusual pattern of the Sa readings.

Table 6: Pearson Correlation Coefficient between Ra and Sa of the machined surface after 20 and 138 mm of cutting length

Cutting Length (mm)	Nano3	AlTiN	TiAlN	TiN	TiSiNext	UNI+
0-20	0.48	0.93	0.55	0.28	0.40	0.72
0-138	0.75	0.82	0.67	0.07	0.55	0.89

To better understand the difference between Ra and Sa they were both graphed against cutting length in Figure 11 to observe their variability. Based on these graphs, UNI+ and AlTiN do appear to be well correlated with very similar trend lines between Ra and Sa. Nano3 also appears well correlated except for a single spike in the Sa data at about 40 mm. This spike is most likely because Sa takes a reading from a larger rectangular area and may have included a defect that wasn't included in the Ra reading. These results are in line with the PCC readings from Table 6, which showed that these three coatings had the strongest relationship. TiAlN and TiSiNext both have a similar trend, but the high variability of the Sa readings causes a difference in the correlation coefficient. This high variability is most likely caused by an issue similar to what caused the Nano3 Sa values to spike. The TiN values showed no real correlation with high variability in the Sa reading along the entire cutting length. Studying these graphs shows that Sa and Ra generally have a good correlation, but Sa has much high variability in its values because it is based on a larger surface area it covered compared to Ra.

Aramcharoen et al. (2008) found similar trends in Ra values, although the values were

smaller due to a lower cutting speed and depth of cut. They also studied TiN and TiAlN coated tools and found that TiN provided a lower surface finish.

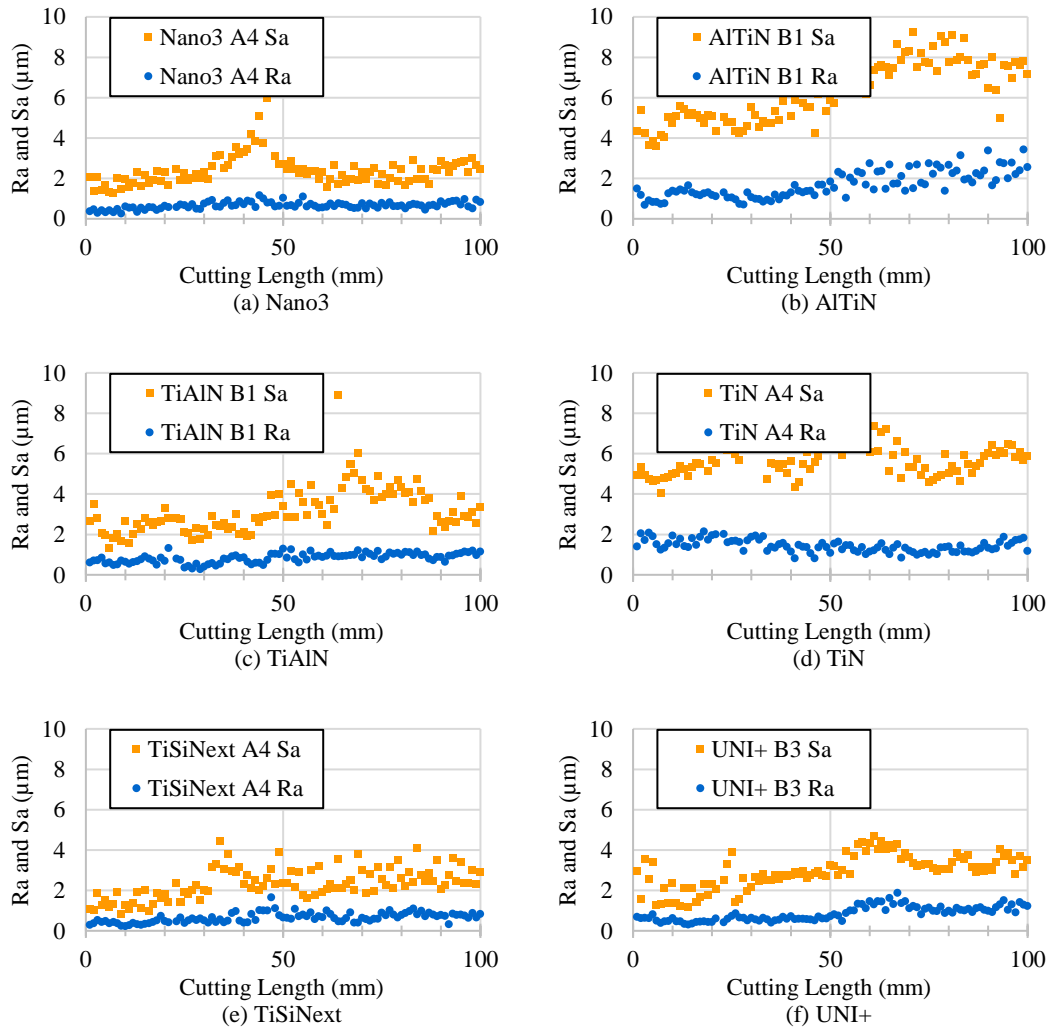


Figure 11: Ra and Sa versus cutting length for coatings. Depth of Cut: 40 μm, Cutting Speed: 40 m/min, Chip Load: 10 μm/flute

5.4. Effect of Tools Coating and Cutting Speed

The effect of cutting speed was studied using Nano3 and UNI+ coated tools. These coatings were selected because they had been the best performing coatings based on the lowest average Ra values across all the tools. All the previous data came from a cutting speed of 40 m/min, a cutting speed of 20 m/min was then completed to study how the lower cutting speed affected surface roughness. The results are shown in Figure 12. The average Ra value for 20 mm of cutting length at 40 m/min cutting speed was 0.455 and 0.426 μm for Nano3 and UNI+ respectively. At 20 m/min of cutting speed the average Ra was 0.244 and 0.241 for Nano3 and UNI+. The higher cutting speed led to higher tool wear which led to a higher surface roughness.

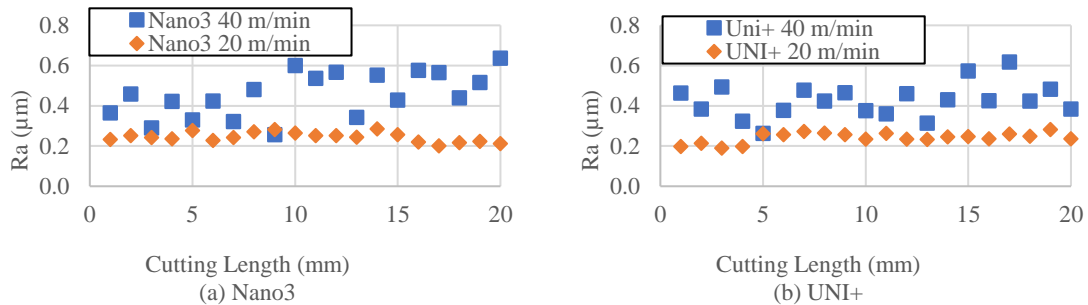


Figure 12: Ra of Machined Channels at Different Cutting Speeds. Depth of Cut: 40 μm , Cutting Speed: 40 m/min and 20 m/min, Chip Load: 10 $\mu\text{m}/\text{flute}$

The equation for theoretical surface roughness is shown in Equation 2. This equation assumes no tool wear and is independent of cutting speed. The increase in surface roughness for the higher cutting speed is likely caused by the increased tool wear that changed the tool geometry. The theoretical surface roughness of the workpiece is 0.15 μm based on the chip load of 10 $\mu\text{m}/\text{flute}$ and concavity angle of 3°. The lowest

single Ra value from the collected data was 0.23 μm but the first data point was taken after 1 mm of cutting length so tool wear should already be affecting the readings.

$$Ra' = \frac{5}{18} f_t \tan \alpha \quad (2)$$

Where:

- Ra' : Theoretical Line Surface Roughness (μm)
- f_t : Chip Load ($\mu\text{m}/\text{flute}$)
- α : Concavity Angle (degrees)

This study selected 20 and 40 m/min cutting speed, 10 $\mu\text{m}/\text{flute}$ chip load, for micromilling in MQL condition. Other researchers performed micromilling H13 tool steel at different milling parameters as described in Table 7. Manso et al. (2020) used a similar cutting speed but had a lower chip load, Aramcharoen et al. (2008) had much lower cutting speed and lower chip load. As a result, the Ra after machining was in the range of 0.1-0.15 μm . Aramcharoen et al. (2009) had Ra values in the ranging from 0.14-0.26 μm after micromilling without cutting fluid. These results are only slightly lower than the results from using a cutting speed of 20 m/min in this experiment which ranged from 0.19-0.29.

Table 7: Machining Parameters of other researchers

Author	Tool Diameter (mm)	Cutting Speed (m/min)	Chip Load ($\mu\text{m}/\text{flute}$)	Cutting Fluid
Manso et al. (2020) [22]	0.4	37.7-57.8	2-5	Dry
Aramcharoen (2008) [21]	0.5	0.3	5	Dry
Aramcharoen (2009) [14]	0.9	0.012-0.216	0.2-3.6	Dry

5.5. Channel Width

The widths of the machined channels were then compared to see if channel width and tool wear had a relationship. The results shown in Figure 13 are the difference from the initial channel width for each tool. To determine if channel width was a reliable form of measurement, only the first 23 mm of cutting length was studied. There should be a linear relationship between the data points with a slight negative trend as the tool coating wears away, making the tool smaller. Instead, it is observed that while some of the tools followed the expected trend relatively well others saw large variation between different tools of the same coating, such as AlTiN A2 and AlTiN A4 in Figure 13b along with all the tools in Figure 13e.

This variation in channel widths is most likely from collecting the channel width using a top-down view of the channels. This led to issues of burrs overlapping the edges of the channels and the exact width being difficult to obtain. There was also a lot of inconsistency in the initial channel width, with a range from 381 to 407 μm . In future studies the channel width should be obtained using a cross section view of the part that may make it more accurate.

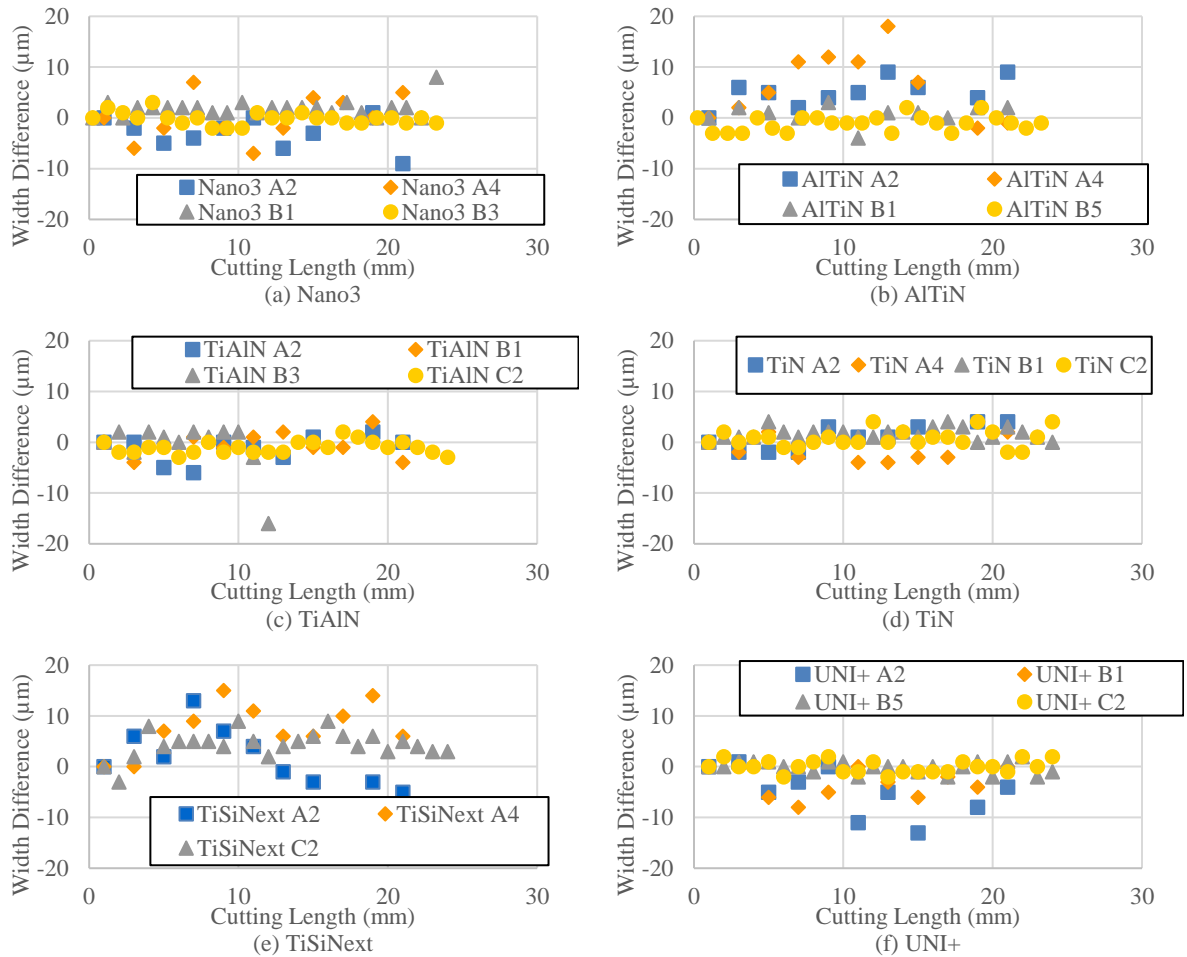


Figure 13: Effects of Coating on Channel Width. Depth of Cut: 40 µm, Cutting Speed: 40 m/min, Chip Load: 10 µm/flute

5.6. Coating Wear

Images of tools of each coating after machining are shown in Figure 14-Figure 20. All tools machined for 23 mm except for uncoated and TiAlN which were machined until reaching 141 mm. All the tools that machined for 23 mm had the coating worn out in a similar fashion, best shown in Figure 20. When the tool tip is worn out, the concavity angle changes from 3° to close to 0°, the tool tip is flattened and rubs along the machined surface. The H13 tool steel BUEs can be seen smearing at the flattened tool surface in

Figure 19. The tool wear is caused by abrasive wear of the coating and spalling of the tungsten carbide cobalt (WC-Co) substrate. The rough surface of the fractured tool surface is evidence of attrition wear [39]. Breaking of large BUEs reveals the rough surface of the fresh tungsten carbide cobalt (WC-Co) structure. This consistency of this wear mechanism shows that the cutting speed was most likely too high leading to the worn-out coating, forming of BUEs on tool edges, and spalling of BUEs with minute amount of cutting tool substrate. All the tools show a similar flat surface at the cutting edge, the evidence of tool rubbing against the workpiece instead of actually cutting. The TiAlN tool, Figure 17, does not show this wear mechanism but it may be from the longer cutting length that wears the coating completely from the cutting edge. The remaining cutting edge appears like that of the uncoated tool which had the same cutting distance. The coating adhesion appears to be good and uniform to approximately 2 μm thick. In their study, Aramcharoen et al. (2008) found the thickness of their coatings to be between 1.38 μm for the TiN coatings up to 1.59 μm thick for the CrTiAlN coating [21]. After a cutting length of 25 mm, they found that the average flank wear of the tools to be between 10 μm for the TiN coated tools up to 30 μm for the AlTiN coated tools, meaning that the coating had worn away and machining was being performed by the tungsten carbide substrate. Manso et al. (2020) found that after 200 mm of cutting length flank wear was around 30 μm on a $\text{\O}0.4$ mm AlTiN coated tool depending on the feed per tooth, while after 1200 mm of cutting length flank wear was nearing 80 μm [22]. These studies show that the tool coating wore away leaving the substrate to perform most of the machining resulting in the high flank wear. This leads to higher tool wear rates and a poorer surface finish on the workpiece. Because

the coating protects the cutting tool it is best practice to only use a tool while the coating is still present on the cutting edge. Technique to reliably detect the useful life of tool coating, however, is yet to be studied.

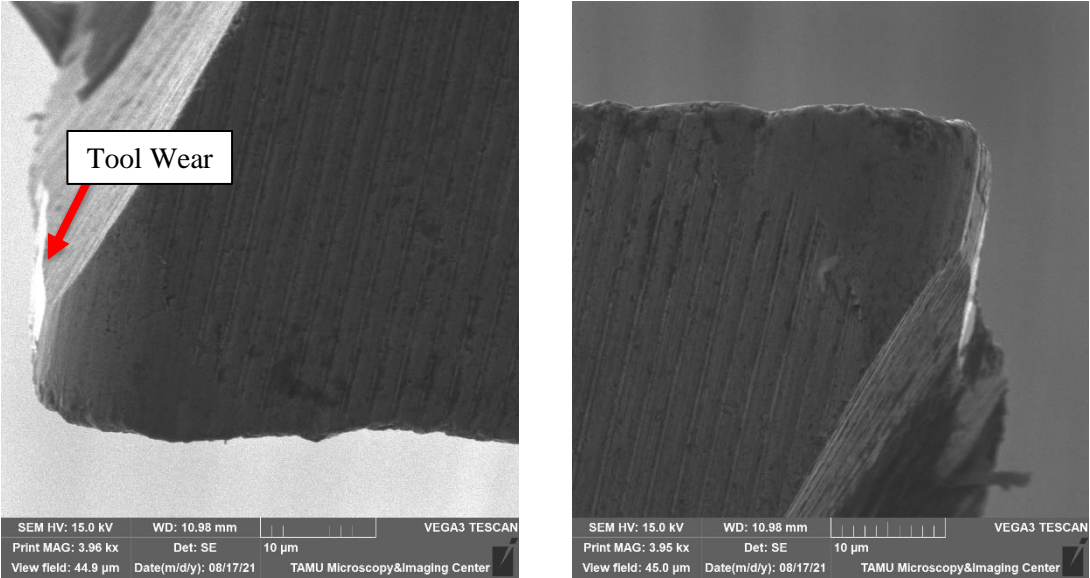


Figure 14: Uncoated cutting edges after machining 141 mm. Depth of Cut: 40 μm , Cutting Speed: 40 m/min, Chip Load: 10 $\mu\text{m}/\text{flute}$

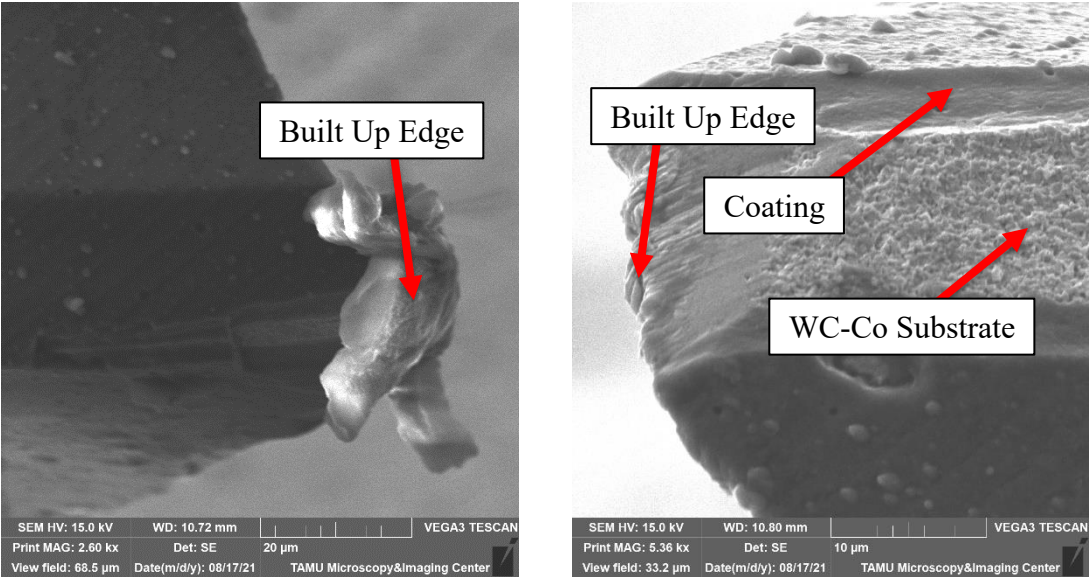


Figure 15: Nano3 Coated cutting edges after machining 23 mm. Depth of Cut: 40 μm , Cutting Speed: 40 m/min, Chip Load: 10 $\mu\text{m}/\text{flute}$

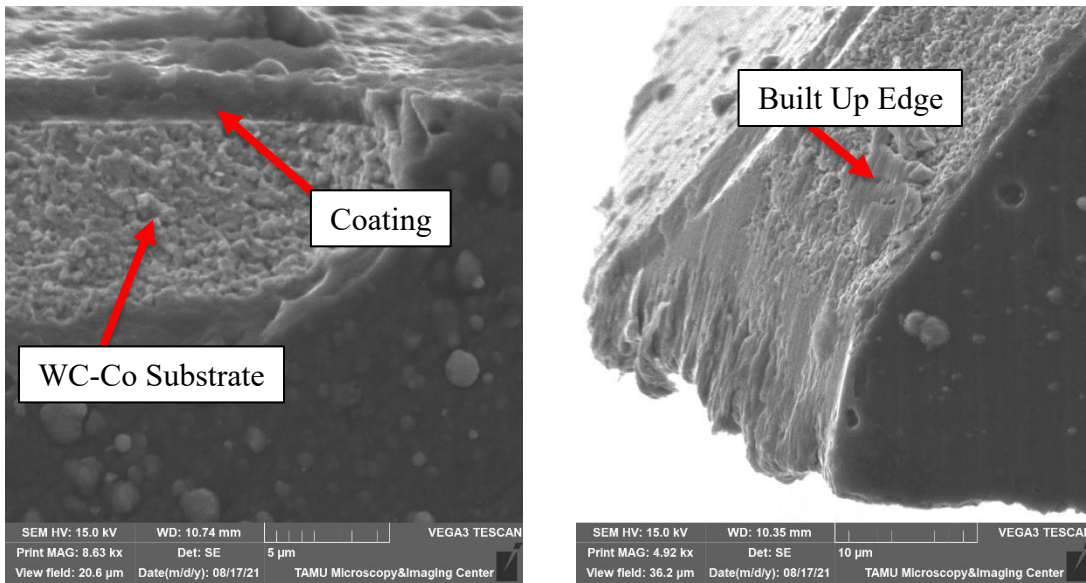


Figure 16: AlTiN Coated cutting edges after machining 23 mm. Depth of Cut: 40 μm, Cutting Speed: 40 m/min, Chip Load: 10 μm/flute

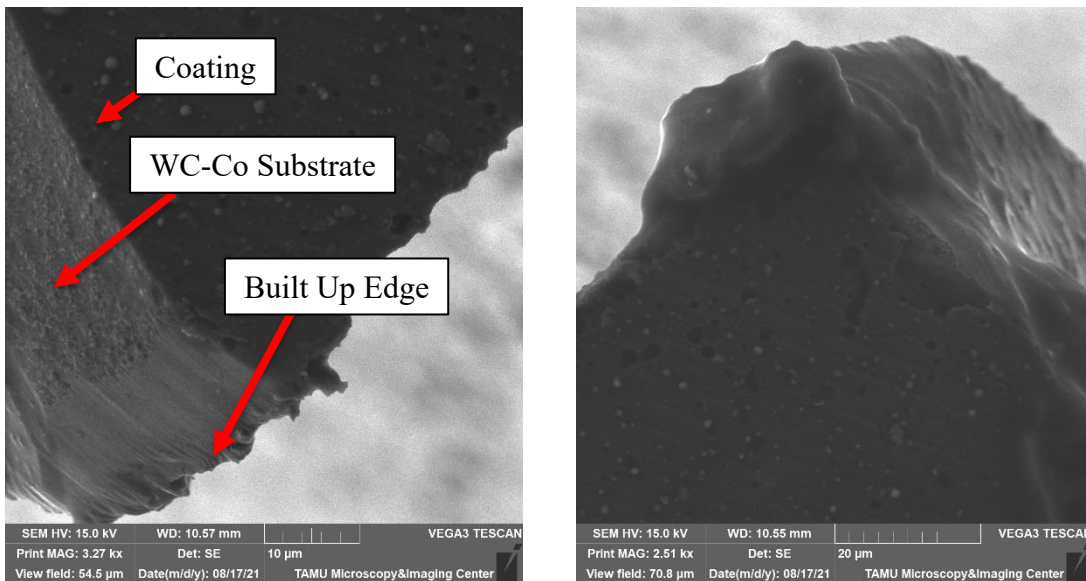


Figure 17: TiAlN Coated cutting edges after machining 141 mm. Depth of Cut: 40 μm, Cutting Speed: 40 m/min, Chip Load: 10 μm/flute

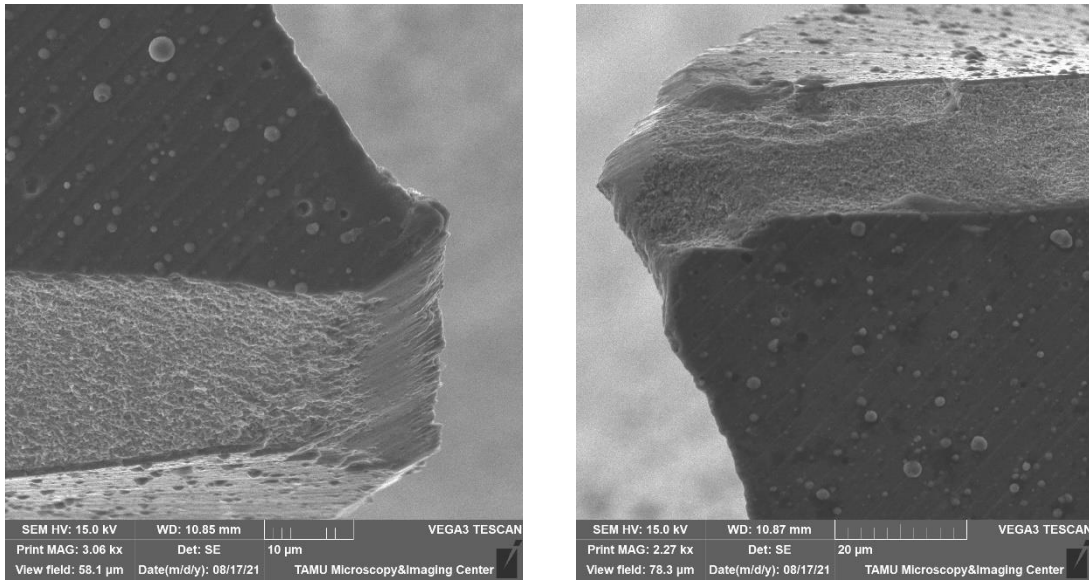


Figure 18: TiN Coated cutting edges after machining 23 mm. Depth of Cut: 40 µm, Cutting Speed: 40 m/min, Chip Load: 10 µm/flute

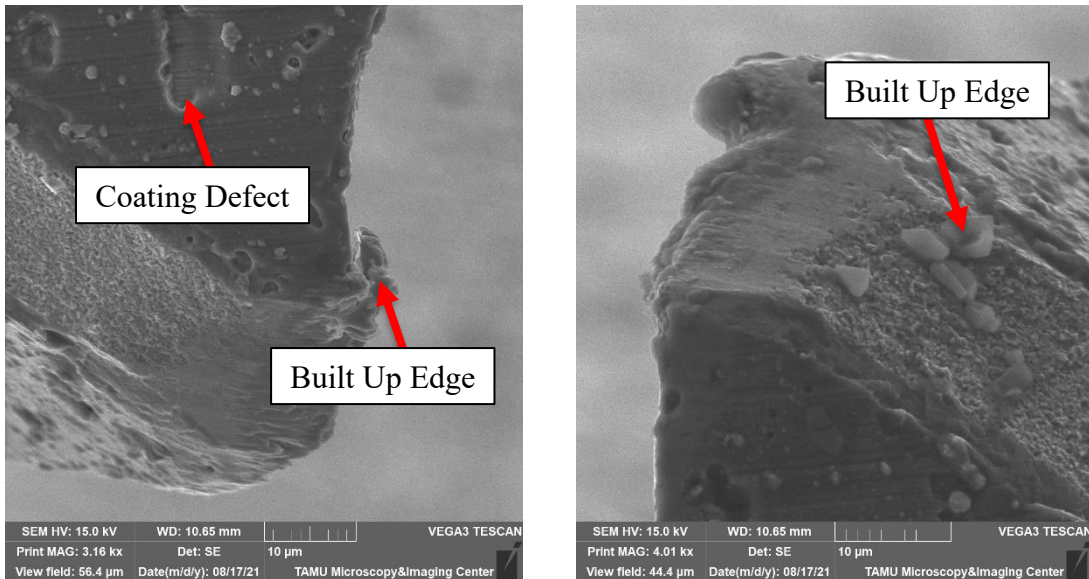


Figure 19: TiSiNext Coated cutting edges after machining 23 mm. Depth of Cut: 40 µm, Cutting Speed: 40 m/min, Chip Load: 10 µm/flute

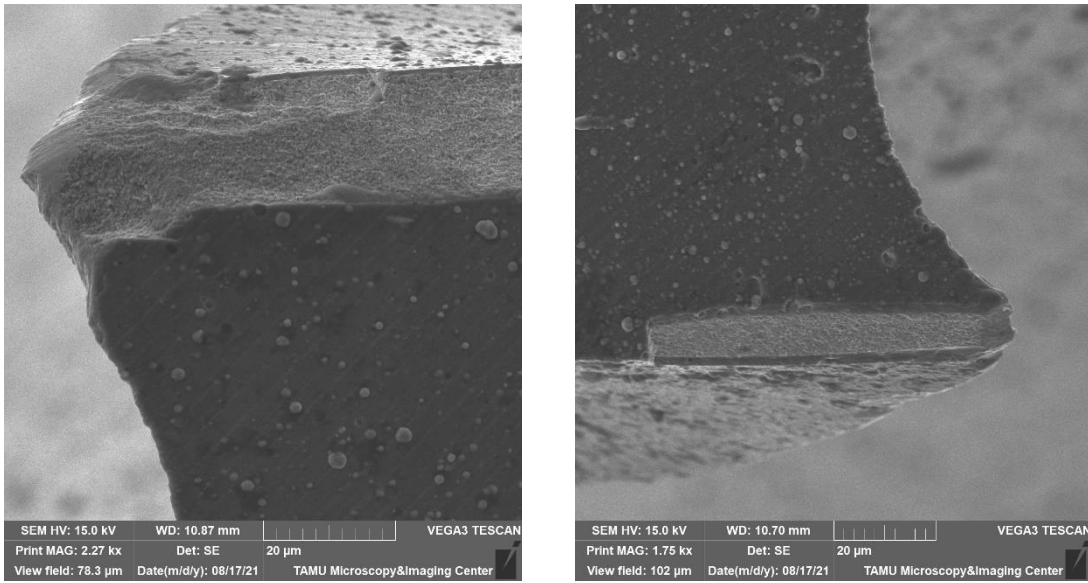


Figure 20: UNI+ Coated cutting edges after machining 23 mm. Depth of Cut: 40 µm, Cutting Speed: 40 m/min, Chip Load: 10 µm/flute

6. CONCLUSIONS AND RECOMMENDATIONS

Micromilling of wrought H13 tool steel was performed using uncoated and tools commercially coated with Nano3, AlTiN, UNI+, TiN, TiSiNext, and TiAlN.

The study showed:

1. Uncoated tool was inferior to the coated tools. The tool wear mechanism was abrasive wear of the coating and spalling of the tungsten carbide cobalt (WC-Co) substrate. The rough surface of the tool surface is evidence of attrition wear.
2. Producing the lowest and most consistent surface finish, tools with Nano3 and UNI+ coatings were the best performing tools when micromilling at 40 μm depth of cut, 40 m/min cutting speed, and 10 μm /flute chip load in MQL conditions.
3. The cutting speed of 40 m/min was too aggressive and caused abrasive and attrition wear of a tool after machining only 23 mm.
4. Channel width was not a viable means of examining tool wear when measured top down. Burrs on both sides of micromilled slots prevented an accurate measurement of channel widths.

Recommendations

- Future study should optimize milling parameters in minimum quantity lubricant to avoid attrition tool wear.
- Since coating functions as a protective layer of a cutting tool, a comprehensive study on coating life and tool life would be useful.
- This work used wrought H13 tool steel, future study should repeat with additively manufactured H13 tool steel.

REFERENCES

- [1] P. Koshy, R. C. Dewes, and D. K. Aspinwall, “High speed end milling of hardened AISI D2 tool steel (~58 HRC),” *Journal of Materials Processing Technology*, vol. 127, no. 2, pp. 266–273, 2002, doi: 10.1016/S0924-0136(02)00155-3.
- [2] A. Bahrami, S. H. M. Anijdan, M. A. Golozar, M. Shamanian, and N. Varahram, “Effects of conventional heat treatment on wear resistance of AISI H13 tool steel,” *Wear*, vol. 258, no. 5–6, pp. 846–851, 2005, doi: 10.1016/j.wear.2004.09.008.
- [3] E. Nas, O. Özbek, F. Bayraktar, and F. Kara, “Experimental and Statistical Investigation of Machinability of AISI D2 Steel Using Electroerosion Machining Method in Different Machining Parameters,” *Advances in Materials Science and Engineering*, vol. 2021, 2021, doi: 10.1155/2021/1241797.
- [4] V. Braga *et al.*, “Microstructural and mechanical aspects of laser metal deposited H13 powder for die repair,” *Materials Today Communications*, vol. 29, no. March, p. 102945, 2021, doi: 10.1016/j.mtcomm.2021.102945.
- [5] H. Deng, Y. Huang, S. Wu, and Y. Yang, “Binder jetting additive manufacturing: Three-dimensional simulation of micro-meter droplet impact and penetration into powder bed,” *Journal of Manufacturing Processes*, vol. 74, no. December 2021, pp. 365–373, 2022, doi: 10.1016/j.jmapro.2021.12.019.
- [6] A. Shad, R. Stache, and A. Rütjes, “Effects of fumed silica flow aids on flowability and packing of metal powders used in Binder-Jetting additive

- manufacturing process,” *Materials and Design*, vol. 212, p. 110253, 2021, doi: 10.1016/j.matdes.2021.110253.
- [7] A. Zavdoveev *et al.*, “Optimization of the pulsed arc welding parameters for wire arc additive manufacturing in austenitic steel applications,” *International Journal of Advanced Manufacturing Technology*, no. 0123456789, 2022, doi: 10.1007/s00170-022-08704-4.
- [8] T. YU, M. CHEN, and Z. WU, “Experimental and numerical study of deposition mechanisms for cold spray additive manufacturing process,” *Chinese Journal of Aeronautics*, vol. 35, no. 2, pp. 276–290, 2022, doi: 10.1016/j.cja.2021.02.002.
- [9] J. S. Park, J. H. Park, M. G. Lee, J. H. Sung, K. J. Cha, and D. H. Kim, “Effect of Energy Input on the Characteristic of AISI H13 and D2 Tool Steels Deposited by a Directed Energy Deposition Process,” *Metallurgical and Materials Transactions A: Physical Metallurgy and Materials Science*, vol. 47, no. 5, pp. 2529–2535, 2016, doi: 10.1007/s11661-016-3427-5.
- [10] J. Y. Jeng and M. C. Lin, “Mold fabrication and modification using hybrid processes of selective laser cladding and milling,” *Journal of Materials Processing Technology*, vol. 110, no. 1, pp. 98–103, 2001, doi: 10.1016/S0924-0136(00)00850-5.
- [11] X. Zhang, W. Cui, W. Li, and F. Liou, “A hybrid process integrating reverse engineering, pre-repair processing, additive manufacturing, and material testing for component remanufacturing,” *Materials*, vol. 12, no. 12, 2019, doi: 10.3390/ma12121961.

- [12] J. Chae, S. S. Park, and T. Freiheit, “Investigation of micro-cutting operations,” *International Journal of Machine Tools and Manufacture*, vol. 46, no. 3–4, pp. 313–332, 2006, doi: 10.1016/j.ijmachtools.2005.05.015.
- [13] F. B. de Oliveira, A. R. Rodrigues, R. T. Coelho, and A. F. de Souza, “Size effect and minimum chip thickness in micromilling,” *International Journal of Machine Tools and Manufacture*, vol. 89, pp. 39–54, 2015, doi: 10.1016/j.ijmachtools.2014.11.001.
- [14] A. Aramcharoen and P. T. Mativenga, “Size effect and tool geometry in micromilling of tool steel,” *Precision Engineering*, vol. 33, no. 4, pp. 402–407, 2009, doi: 10.1016/j.precisioneng.2008.11.002.
- [15] T. Wang, X. Wu, G. Zhang, B. Xu, Y. Chen, and S. Ruan, “Theoretical study on the effects of the axial and radial runout and tool corner radius on surface roughness in slot micromilling process,” *International Journal of Advanced Manufacturing Technology*, vol. 108, no. 5–6, pp. 1931–1944, 2020, doi: 10.1007/s00170-020-05492-7.
- [16] S. N. B. Oliaei and Y. Karpaz, “Influence of tool wear on machining forces and tool deflections during micro milling,” *International Journal of Advanced Manufacturing Technology*, vol. 84, no. 9–12, pp. 1963–1980, 2016, doi: 10.1007/s00170-015-7744-4.
- [17] A. Davoudinejad, D. Li, Y. Zhang, and G. Tosello, “Effect of progressive tool wear on the functional performance of micro milling process of injection molding

- tool,” in *Procedia CIRP*, 2020, vol. 87, pp. 159–163. doi:
10.1016/j.procir.2020.02.031.
- [18] A. Muhammad, M. K. Gupta, T. Mikołajczyk, D. Y. Pimenov, and K. Giasin, “Effect of tool coating and cutting parameters on surface roughness and burr formation during micromilling of inconel 718,” *Metals (Basel)*, vol. 11, no. 1, pp. 1–18, 2021, doi: 10.3390/met11010167.
- [19] H. Hassanpour, M. H. Sadeghi, H. Rezaei, and A. Rasti, “Experimental Study of Cutting Force, Microhardness, Surface Roughness, and Burr Size on Micromilling of Ti6Al4V in Minimum Quantity Lubrication,” *Materials and Manufacturing Processes*, vol. 31, no. 13, pp. 1654–1662, 2016, doi:
10.1080/10426914.2015.1117629.
- [20] A. Varghese, P. K. Maurya, V. Kulkarni, and S. S. Joshi, “Experimental investigation of the correlation between surface roughness and tool-life in micromilling,” *Advances in Materials and Processing Technologies*, vol. 5, no. 1, pp. 67–77, 2019, doi: 10.1080/2374068X.2018.1524255.
- [21] A. Aramcharoen, P. T. Mativenga, S. Yang, K. E. Cooke, and D. G. Teer, “Evaluation and selection of hard coatings for micro milling of hardened tool steel,” *International Journal of Machine Tools and Manufacture*, vol. 48, no. 14, pp. 1578–1584, 2008, doi: 10.1016/j.ijmachtools.2008.05.011.
- [22] C. S. Manso, S. Thom, E. Uhlmann, C. L. F. de Assis, and E. G. del Conte, “Investigation of micromilled tool steel H13 using tungsten carbide micro-end

- mills,” *International Journal of Advanced Manufacturing Technology*, vol. 107, no. 3–4, pp. 1179–1189, 2020, doi: 10.1007/s00170-020-05075-6.
- [23] E. Vazquez, J. Gomar, J. Ciurana, and C. A. Rodríguez, “Analyzing effects of cooling and lubrication conditions in micromilling of Ti6Al4V,” *Journal of Cleaner Production*, vol. 87, no. 1, pp. 906–913, 2015, doi: 10.1016/j.jclepro.2014.10.016.
- [24] M. Ziberov, M. B. da Silva, M. Jackson, and W. N. P. Hung, “Effect of Cutting Fluid on Micromilling of Ti-6Al-4V Titanium Alloy,” *Procedia Manufacturing*, vol. 5, no. 2003, pp. 332–347, 2016, doi: 10.1016/j.promfg.2016.08.029.
- [25] J. S. Park *et al.*, “Effect of heat treatment on the characteristics of tool steel deposited by the directed energy deposition process,” *Metals and Materials International*, vol. 22, no. 1, pp. 143–147, 2016, doi: 10.1007/s12540-016-5372-7.
- [26] M. A. Sadiq, N. M. Hoang, N. Valencia, S. Obeidat, and W. N. P. Hung, “Experimental study of micromilling selective laser melted Inconel 718 superalloy,” *Procedia Manufacturing*, vol. 26, pp. 983–992, 2018, doi: 10.1016/j.promfg.2018.07.129.
- [27] Y. Bai, A. Chaudhari, and H. Wang, “Investigation on the microstructure and machinability of ASTM A131 steel manufactured by directed energy deposition,” *Journal of Materials Processing Technology*, vol. 276, no. August 2019, p. 116410, 2020, doi: 10.1016/j.jmatprotec.2019.116410.

- [28] A. Colpani, A. Fiorentino, E. Ceretti, and A. Attanasio, "Tool wear analysis in micromilling of titanium alloy," *Precision Engineering*, vol. 57, no. March, pp. 83–94, 2019, doi: 10.1016/j.precisioneng.2019.03.011.
- [29] L. C. Silva and M. B. da Silva, "Investigation of burr formation and tool wear in micromilling operation of duplex stainless steel," *Precision Engineering*, vol. 60, no. August, pp. 178–188, 2019, doi: 10.1016/j.precisioneng.2019.08.006.
- [30] M. H. M. Dib, J. G. Duduch, and R. G. Jasinevicius, "Minimum chip thickness determination by means of cutting force signal in micro endmilling," *Precision Engineering*, vol. 51, no. April 2017, pp. 244–262, 2018, doi: 10.1016/j.precisioneng.2017.08.016.
- [31] Q. S. Bai, K. Yang, Y. C. Liang, C. L. Yang, and B. Wang, "Tool runout effects on wear and mechanics behavior in microend milling," *Journal of Vacuum Science & Technology B: Microelectronics and Nanometer Structures*, vol. 27, no. 3, p. 1566, 2009, doi: 10.1116/1.3058729.
- [32] M. A. Câmara, A. M. Abrão, J. C. Campos Rubio, G. C. D. Godoy, and B. S. Cordeiro, "Determination of the critical undeformed chip thickness in micromilling by means of the acoustic emission signal," *Precision Engineering*, vol. 46, pp. 377–382, 2016, doi: 10.1016/j.precisioneng.2016.06.007.
- [33] M. C. Gomes, M. B. da Silva, and M. A. V. Duarte, "Experimental study of micromilling operation of stainless steel," *International Journal of Advanced Manufacturing Technology*, vol. 111, no. 11–12, pp. 3123–3139, 2020, doi: 10.1007/s00170-020-06232-7.

- [34] “Performance Micro Tools.” Janesville, WI. [Online]. Available: <http://www.pmtnow.com/>
- [35] “Swiss-Tek Coating, Inc.” Pewaukee, WI. [Online]. Available: <http://www.swiss-tekcoatings.com/>
- [36] J. Zhu, Z. Zhang, and J. Xie, “Improving strength and ductility of H13 die steel by pre-tempering treatment and its mechanism,” *Materials Science and Engineering A*, vol. 752, no. February, pp. 101–114, 2019, doi: 10.1016/j.msea.2019.02.085.
- [37] J. C. Lee, H. J. Kang, W. S. Chu, and S. H. Ahn, “Repair of Damaged Mold Surface by Cold-Spray Method,” *CIRP Annals - Manufacturing Technology*, vol. 56, no. 1, pp. 577–580, 2007, doi: 10.1016/j.cirp.2007.05.138.
- [38] G. Li, A. Zhang, Q. Zhang, D. Wu, and C. Zhan, “Pearson Correlation Coefficient-based performance enhancement of Broad Learning System for stock price prediction,” *IEEE Transactions on Circuits and Systems II: Express Briefs*, May 2022, doi: 10.1109/TCSII.2022.3160266.
- [39] A. E. Diniz, Á. R. Machado, and J. G. Corrêa, “Tool wear mechanisms in the machining of steels and stainless steels,” *International Journal of Advanced Manufacturing Technology*, vol. 87, no. 9–12, pp. 3157–3168, Dec. 2016, doi: 10.1007/s00170-016-8704-3.

APPENDIX A

MICROMILLING PROCEDURE

1. Insert workpiece into compound vise
2. Use bullet level for making a flat surface as shown in *Figure 21*

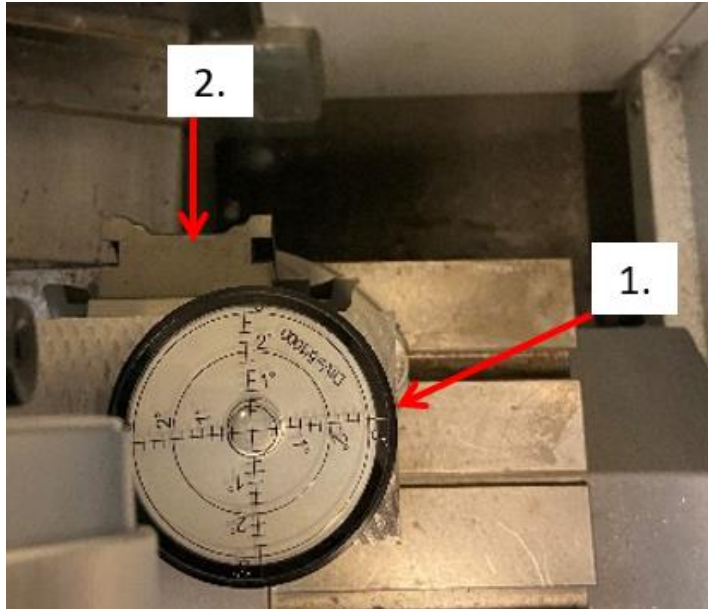


Figure 21: Using a bullet level (Top View) 1) Bullet Level and 2) Compound Vise

3. Verify the flat surface using an indicator mounted to the spindle as shown in

Figure 22

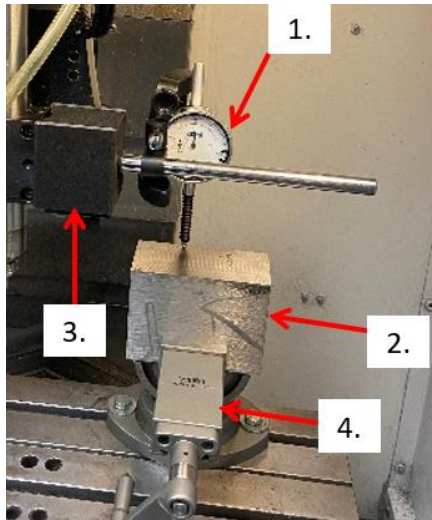


Figure 22: Using Indicator Mounted to the Spindle 1) Indicator, 2) Workpiece, 3) Magnetic Mounting Base, and 4) Compound Vise

4. Secure the tool in the collet
5. Set X and Y axis tool offsets visually at the origin of the workpiece
6. Secure multimeter probe to tool and workpiece
7. Turn on multimeter to measure for resistance
8. Slowly lower the tool until the multimeter beeps showing that the tool is in contact with the workpiece
9. Set the Z axis offset
10. Turn on the micromist
11. Run program shown in Appendix C

APPENDIX B

TOOL AND PART OFFSETS FOR MICROMILLING

This method replaces steps 6-9 in Appendix A

1. Tape thin aluminum sheet to gage block
2. Put a mark on the aluminum sheet where the tool will make contact
3. Place gage block on the workpiece
4. Aim laser height gage at the mark
5. Zero the laser height gage
6. Remove gage block to measure the height of the aluminum sheet
7. Note the height of the aluminum sheet
8. Place gage block back on the workpiece aligned so that the tool will contact the mark
9. Aim the laser height gage on the aluminum sheet in a non-marked location as shown in Figure 23

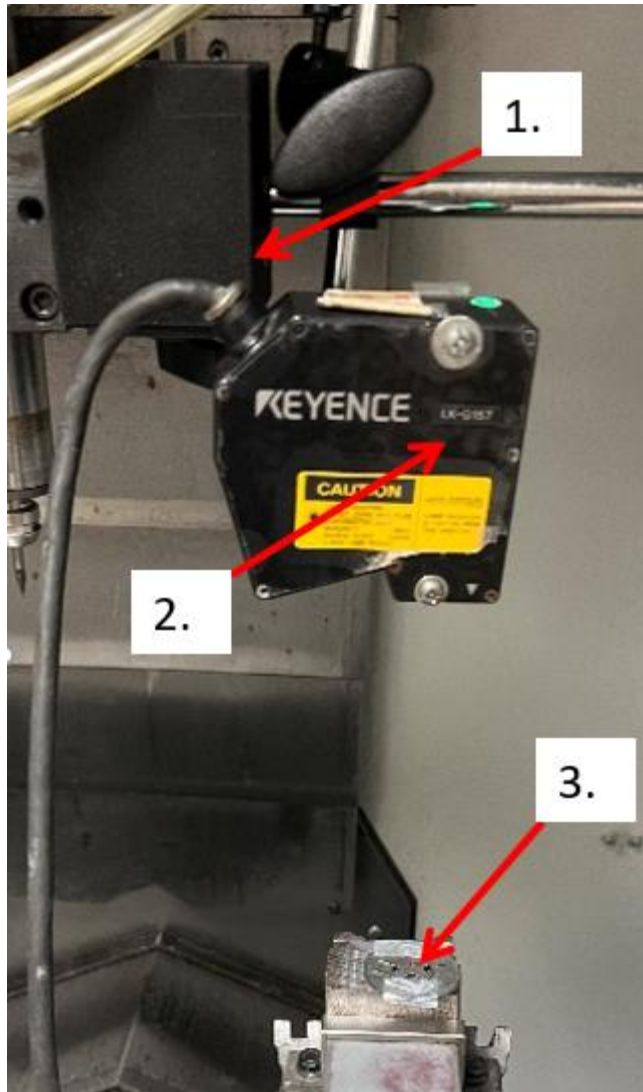


Figure 23: Using Laser Height Gage 1) Magnetic Mounting Base, 2) Laser Height Gage, and 3) Washer with aluminum sheet

10. Zero the laser height gage

11. Slowly lower the tool until the height of the aluminum sheet changes

12. Set the Z axis offset

13. Subtract the height of the aluminum sheet and gage block noted earlier



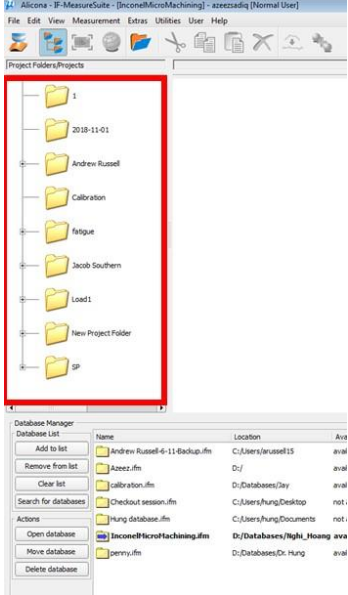
APPENDIX C

NC CODES

```
%  
O66669  
(SS316L Russell H13 Block 2 6/9 15:00)  
( FEATURECAM HAAS OM2 MILLING )  
  
N35 ( OPERATION= SLOT GROOVE1 )  
N40 ( TOOL: T1 = 0.4 mm )  
N45 G01 G17 G21 G40 G90 G94  
N50 T1 M06  
N55 G54 X-3.0 Y-3.0 Z3.0 S31830 F637.0 M03  
N70 (Slot 1)  
N75 Z-0.04  
N80 X1.0  
N85 Y50.0  
N90 Z2.0  
N95 (Slot 2)  
N100 X1.5 Y-3.0  
N110 Z-0.04  
N115 Y50.0  
N120 Z2.0  
N125 (Slot 3)  
N130 X2.0 Y-3.0  
N140 Z-0.04  
N145 Y50.0  
N150 Z2.0  
N125 (Slot 4)  
N130 X2.5 Y-3.0  
N140 Z-0.04  
N145 Y50.0  
N150 Z2.0  
N125 (Slot 5)  
N130 X3.0 Y-3.0  
N140 Z-0.04  
N145 Y50.0  
N150 Z2.0  
  
N215 X3.0 Y-3.0  
  
N400 G53 G49 Z0 M09  
N410 M30
```

APPENDIX D

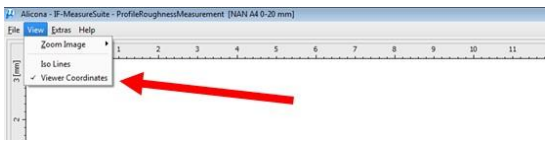
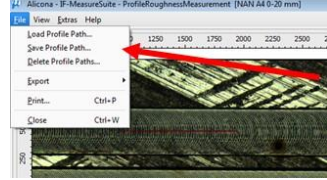

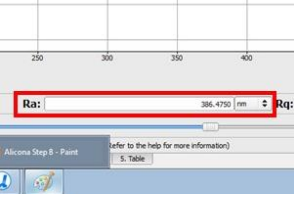
PROCEDURE USING ALICONA INFINITE FOCUS MICROSCOPE

<p>1. Open IF Measurement Suite</p>																									
<p>2. Log in to User Name. You can use your own or log in with an existing one. It does not matter as long as you use the same one every time you log in.</p>																									
<p>3. Open Folder where your files are saved.</p>	 <table border="1"><thead><tr><th>name</th><th>Location</th><th>Avai</th></tr></thead><tbody><tr><td>Andrew Russell-6-11-Backup.ifm</td><td>C:\Users\arussell15</td><td>avail</td></tr><tr><td>Azeczr.ifm</td><td>D:/</td><td>avail</td></tr><tr><td>calibration.ifm</td><td>D:\Databases\Day</td><td>avail</td></tr><tr><td>Checkout session.ifm</td><td>C:\Users\hung\Desktop</td><td>not</td></tr><tr><td>Hung database.ifm</td><td>C:\Users\hung\Documents</td><td>not</td></tr><tr><td>Inconel@MicroMachining.ifm</td><td>D:\Databases\Ngph_Hoang ava</td><td>avail</td></tr><tr><td>penny.ifm</td><td>D:\Databases\Dr. Hung</td><td>avail</td></tr></tbody></table>	name	Location	Avai	Andrew Russell-6-11-Backup.ifm	C:\Users\arussell15	avail	Azeczr.ifm	D:/	avail	calibration.ifm	D:\Databases\Day	avail	Checkout session.ifm	C:\Users\hung\Desktop	not	Hung database.ifm	C:\Users\hung\Documents	not	Inconel@MicroMachining.ifm	D:\Databases\Ngph_Hoang ava	avail	penny.ifm	D:\Databases\Dr. Hung	avail
name	Location	Avai																							
Andrew Russell-6-11-Backup.ifm	C:\Users\arussell15	avail																							
Azeczr.ifm	D:/	avail																							
calibration.ifm	D:\Databases\Day	avail																							
Checkout session.ifm	C:\Users\hung\Desktop	not																							
Hung database.ifm	C:\Users\hung\Documents	not																							
Inconel@MicroMachining.ifm	D:\Databases\Ngph_Hoang ava	avail																							
penny.ifm	D:\Databases\Dr. Hung	avail																							


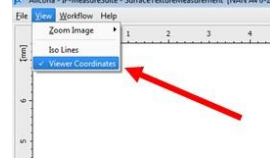
<p>4. Open the file you want to measure</p>	
---	--

For Measuring Ra

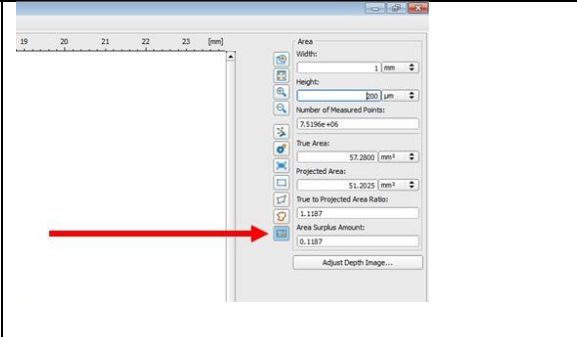
<p>1. Record the image of calibration block using the same zoom level used for your part readings (Calibration block used was Mitutoyo Standard Serial No. 348451205)</p>	
<p>2. Save to the same project as the rest of your pictures</p>	
<p>3. Open in ProfileRoughnessMeasurement</p>	
<p>4. Either use a saved profile path or create a new profile path that you will save</p>	
<p>5. Put Lc to manual and adjust until the Ra value matches the Ra value on the calibration block</p>	

6. Record the number to use when measuring Ra for your part	
7. Select <i>View>Viewer Coordinates</i> in order to see the coordinates at your mouse cursor	
8. Use the profile used for calibration by selecting <i>File>Load Profile Path...</i>	
9. To get an accurate Ra reading use a calibrated Lc value. To put in calibrated value select <i>Manual</i> then enter the calibrated value.	
10. Record the Ra value	

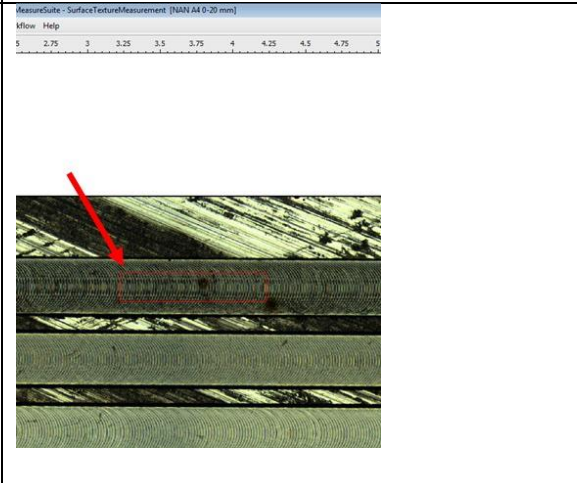
For Measuring Sa

1. Select SurfaceTextureMeasurement for Sa	
2. Select <i>View>Viewer Coordinates</i> to see the coordinates of the mouse cursor	

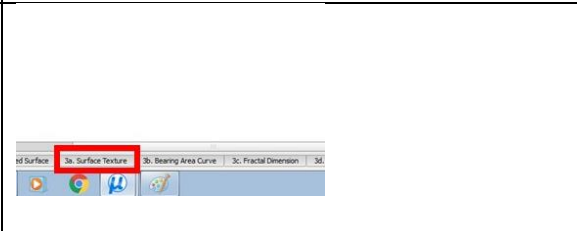
3. Select *Select Fixed Rectangle* and enter your desired width and height.



4. Click the part to place the rectangle where desired



5. Select *Surface Texture* to read Sa value



6. Record the Sa value

